Metabolic Engineering 68 (2021) 68–85

Contents lists available at ScienceDirect

Metabolic Engineering

journal homepage: www.elsevier.com/locate/meteng

A quantitative metabolic analysis reveals *Acetobacterium woodii* as a flexible and robust host for formate-based bioproduction

Christian Simon Neuendorf [a], Gabriel A. Vignolle [a], Christian Derntl [a], Tamara Tomin [b], Katharina Novak [a], Robert L. Mach [a], Ruth Birner-Grünberger [b,c], Stefan Pflügl [a,*]

[a] Technische Universität Wien, Institute for Chemical, Environmental and Bioscience Engineering, Research Area Biochemical Engineering, Gumpendorfer Straße 1a, 1060, Vienna, Austria
[b] Technische Universität Wien, Institute for Chemical Technologies and Analytics, Research Group Bioanalytics, Getreidemarkt 9, 1060, Vienna, Austria
[c] Medical University of Graz, Diagnostic and Research Institute of Pathology, Center for Medical Research, Stiftingtalstrasse 24, 8036, Graz, Austria

ARTICLE INFO

Keywords:
Formate bioeconomy
Acetogens
Substrate co-utilization
Mixed gas fermentation
Continuous fermentation
Metabolic modelling and -omics analysis

ABSTRACT

Cheap and renewable feedstocks such as the one-carbon substrate formate are emerging for sustainable production in a growing chemical industry. We investigated the acetogen *Acetobacterium woodii* as a potential host for bioproduction from formate alone and together with autotrophic and heterotrophic co-substrates by quantitatively analyzing physiology, transcriptome, and proteome in chemostat cultivations in combination with computational analyses. Continuous cultivations with a specific growth rate of 0.05 h^{-1} on formate showed high specific substrate uptake rates (47 mmol g^{-1} h^{-1}). Co-utilization of formate with H_2, CO, CO_2 or fructose was achieved without catabolite repression and with acetate as the sole metabolic product. A transcriptomic comparison of all growth conditions revealed a distinct adaptation of *A. woodii* to growth on formate as 570 genes were changed in their transcript level. Transcriptome and proteome showed higher expression of the Wood-Ljungdahl pathway during growth on formate and gaseous substrates, underlining its function during utilization of one-carbon substrates. Flux balance analysis showed varying flux levels for the WLP (0.7–16.4 mmol g^{-1} h^{-1}) and major differences in redox and energy metabolism. Growth on formate, H_2/CO_2, and formate + H_2/CO_2 resulted in low energy availability (0.20–0.22 ATP/acetate) which was increased during co-utilization with CO or fructose (0.31 ATP/acetate for formate + H_2/CO/CO_2, 0.75 ATP/acetate for formate + fructose). Unitrophic and mixotrophic conversion of all substrates was further characterized by high energetic efficiencies. *In silico* analysis of bioproduction of ethanol and lactate from formate and autotrophic and heterotrophic co-substrates showed promising energetic efficiencies (70–92%). Collectively, our findings reveal *A. woodii* as a promising host for flexible and simultaneous bioconversion of multiple substrates, underline the potential of substrate co-utilization to improve the energy availability of acetogens and encourage metabolic engineering of acetogenic bacteria for the efficient synthesis of bulk chemicals and fuels from sustainable one carbon substrates.

1. Introduction

En route to a circular bioeconomy, industrial biotechnology becomes a key technology to achieve the United Nations sustainable development goals (Arora and Mishra, 2019) and reduce human-made CO_2 emissions (Köpke and Simpson, 2020). However, to meet the rising global demand for chemicals and fuels (Panich et al., 2021), cheap and sustainable feedstocks are needed for industrial bioproduction.

One-carbon substrates and H_2 are emerging as promising alternatives to traditional, agro-based biotechnological feedstocks. Currently, gaseous carbon and energy sources (CO_2, CO, H_2) are available from large point sources (e.g. steel mills) (Köpke and Simpson, 2020; Novak et al., 2021) and can be obtained via gasification of solid municipal waste or residual biomass (Liew et al., 2016). Moreover, bioproduction of ethanol from CO via gas fermentation has already been commercialized (Vees et al., 2020).

* Corresponding author.
E-mail addresses: christian.neuendorf@tuwien.ac.at (C.S. Neuendorf), gabriel.vignolle@tuwien.ac.at (G.A. Vignolle), christian.derntl@tuwien.ac.at (C. Derntl), tamara.tomin@tuwien.ac.at (T. Tomin), katharinanovak.kn@gmail.com (K. Novak), robert.mach@tuwien.ac.at (R.L. Mach), ruth.birner-gruenberger@tuwien.ac.at (R. Birner-Grünberger), stefan.pfluegl@tuwien.ac.at (S. Pflügl).

https://doi.org/10.1016/j.ymben.2021.09.004
Received 14 June 2021; Received in revised form 30 August 2021; Accepted 15 September 2021
Available online 16 September 2021

In the future, circular carbon economies are anticipated to be based on feedstocks obtained from renewable energy (e.g. wind, solar) and CO_2 as abundantly available carbon source (Claassens et al, 2018, 2019; Cotton et al., 2020; Yishai et al., 2016). At this point, CO_2 might be directly captured and concentrated from air (Chatterjee and Huang, 2020; Fasihi et al., 2019; Realmonte et al., 2019).

CO, H_2 and formate have been described as suitable microbial electron donors and are therefore promising mediators between chemical feedstock production and utilization for bioproduction (Boone et al., 1989; Diender et al., 2015). The small one-carbon compound formate is particularly interesting in this context as it can be efficiently produced from CO_2 via electrochemical reduction, hydrogenation and photoreduction (Yishai et al., 2016). Consequently, formate may serve as a chemical energy storage system for excess electricity in the future. While CO and H_2 can also be produced electrochemically or via water hydrolysis with promising efficiencies (Haas et al., 2018; Hardt et al., 2021), formate has several advantages as a substrate compared to the direct utilization of gaseous feedstocks. In contrast to gas fermentations which are typically limited by the gas-liquid mass transfer (Van Hecke et al., 2019), formate is completely miscible with water and can be directly added to the cultivation medium. In addition, the transport and storage of gaseous substrates such as H_2 and CO is challenging due to their high reactivity and toxicity (Cotton et al., 2020; Karmann et al., 2017). Interestingly, the interconversion of H_2, CO and CO_2 to formate by acetogenic bacteria could additionally provide a solution for storage of H_2 (Müller, 2019; Schuchmann and Müller, 2013; Schwarz et al., 2020; Schwarz and Müller, 2020). In the future, formate may be produced in Power-to-X (P2X) approaches. Therefore, formate supply and prices may correlate with the availability of electricity (Li et al., 2012; Yishai et al., 2016).

Currently, several natural and metabolically engineered formatotrophs are investigated for their applicability in formate-based bioproduction. An important criterion for potential microbial hosts is the amount of energy of the substrate that is retained in the product (i.e. energy efficiency) (Claassens et al., 2019). Natural formatotrophs such as *Pseudomonas* species and *Cupriavidus necator* suffer from low energy efficiency on formate, which in turn limits product yields (Claassens et al., 2020; Goldberg et al., 1976). Hence, the metabolic engineering of *Escherichia coli* and *Saccharomyces cerevisiae* for growth on formate focused on efficient assimilation routes such as the reductive glycine pathway (rGLY) (Gonzalez de la Cruz et al., 2019; Kim et al., 2020). Out of all engineered and natural formatotrophs, acetogens show the highest energy efficiency for formate assimilation (Cotton et al., 2020). Acetogens are strictly anaerobic bacteria that utilize the Wood-Ljungdahl Pathway (WLP) and an interlinked redox balancing system for the growth on a variety of one-carbon substrates (Schuchmann and Müller, 2014). The model acetogen *Acetobacterium woodii* utilizes the four one-carbon sources CO, CO_2, formate and methanol (Balch et al., 1977; Bertsch and Müller, 2015a; Kremp et al., 2018; Moon et al., 2021) and is considered for industrial production of the platform chemical acetate from gaseous substrates (Demler and Weuster-Botz, 2011; Kantzow et al., 2015; Novak et al., 2021). Its suitable substrate spectrum and energy-efficient metabolism make *A. woodii* a promising microbial platform organism for sustainable bioprocesses.

In the future, formate may either serve as the main carbon source or as a supplementary substrate in flexible bioprocesses. The co-utilization of formate with other carbon and energy sources such as carbohydrates might offer advantages compared to the use of one-carbon substrates. In addition to higher carbon conversion efficiencies, mixotrophic substrate utilization might be used as a strategy to improve bioenergetics in acetogens single substrates (Jones et al., 2016; Maru et al., 2018; Molitor et al., 2017). Notably, mixotrophic utilization of carbohydrates and gaseous substrates is easily achieved by some acetogens such as *A. woodii* (Braun and Gottschalk, 1981). In addition, the future bioeconomy needs to react flexibly to fluctuating energy and substrate availabilities (Blank et al., 2020; Liew et al., 2016; Wendisch et al., 2016; Yishai et al., 2016). Therefore, co-utilization of substrates and robust process performance with varying substrate supply are desirable.

In this study, we aimed to obtain a quantitative understanding of unitrophic and mixotrophic formate utilization by *A. woodii* to evaluate its potential for formate-based bioproduction. To that end, chemostat cultivations were used to study single substrate (formate, H_2/CO_2 and fructose) utilization on a physiological, transcriptomic and proteomic level. Additionally, we tested whether *A. woodii* can co-utilize formate with gaseous (H_2/CO_2 and $H_2/CO/CO_2$) and heterotrophic (fructose) substrates. Transcriptome and proteome data together with metabolic modelling revealed a high flexibility and robustness of *A. woodii* to utilize multiple substrates simultaneously. Metabolic modelling further highlighted how intracellular energy availability can be controlled by substrate co-utilization. Finally, we discuss the energetic efficiency and strategies for formate-based bioproduction of novel products with *A. woodii*.

2. Material and methods

2.1. Bacterial strain

Acetobacterium woodii DSM1030 was used in all experiments. For cryo-preservation, cell suspensions supplemented with a final sucrose concentration of 125 g L^{-1} were stored at −80 °C.

2.2. Growth medium

For shaken cultivation in serum bottles, cells were grown on a phosphate-buffered medium as previously described (Novak et al., 2021). The medium contained per liter: 1 g NH_4Cl, 2 g yeast extract, 3.47 g NaCl, 0.1 g $MgSO_4 \cdot 7\ H_2O$, 1.76 g KH_2PO_4, 8.44 g K_2HPO_4, 0.5 g cysteine-HCl·H_2O, 0.25 mL sodium resazurin (0.2% w/v), 20 mL adapted trace element solution DSMZ141 and 10 mL vitamin solution DSMZ 141. The vitamin solution from medium recipe DSMZ 141 contained per liter: 2 mg Biotin, 2 mg folic acid, 10 mg pyridoxine-HCl, 5 mg thiamine-HCl, 5 mg riboflavin, 5 mg nicotinic acid, 5 mg D-Ca-pantothenate, 0.1 mg vitamin B_{12}, 5 mg p-Aminobenzoic acid and 5 mg Lipoic acid. The adapted trace element solution based on DSMZ141 contained per liter: 1.5 g nitrilotriacetic acid, 3 g $MgSO_4 \cdot 7\ H_2O$, 0.5 g $MnSO_4 \cdot\ H_2O$, 1 g NaCl, 0.1 g $FeSO_4 \cdot 7\ H_2O$, 0.152 g $Co(II)Cl_2 \cdot 6\ H_2O$, 0.1 g $CaCl_2 \cdot 2\ H_2O$, 0.18 g $ZnSO_4 \cdot 7\ H_2O$, 0.01 g $CuSO_4 \cdot 5\ H_2O$, 0.02 g $KAl(SO_4)_2 \cdot 12\ H_2O$, 0.01 g boric acid, 0.01 g $Na_2MoO_4 \cdot 2\ H_2O$, 0.033 g $Ni(II)SO_4 \cdot 6\ H_2O$, 0.3 mg $Na_2SeO_3 \cdot 5\ H_2O$ and 0.4 mg $Na_2WO_4 \cdot 2\ H_2O$. Formate or fructose were added from anaerobic stocks with concentrations of 230 g $^{L-1}$ or 250 g L^{-1}, respectively. The pH of the medium for serum bottle cultivation was adjusted to 7.2 with 5 M KOH unless stated otherwise. The medium composition was adapted for bioreactor cultivations: There, the amount of vitamin and trace element solution were doubled, Ca-pantothenate was added to a final concentration of 1 mg L^{-1} (Godley et al., 1990) and $FeSO_4 \cdot 7\ H_2O$ to a final concentration of 26.9 mg L^{-1} (Demler and Weuster-Botz, 2011). The phosphate salt concentrations were reduced to 0.33 g L^{-1} KH_2PO_4 and 0.45 g L^{-1} K_2HPO_4 and the pH of the medium was adjusted to 7.0 with 5 M KOH. Antifoam Struktol SB2020 (Schill und Seilacher, Hamburg, Germany) was added to the medium in a ratio of 1:5,000 (v/v).

2.3. Growth conditions

For growth of pre-cultures and small-scale batch cultivations, cells were grown in 125 mL serum bottles using 50 mL medium. All serum bottle cultures were incubated at 30 °C and 200 rpm in a rotary shaker (Infors AG, Bottmingen, Switzerland). The headspace of the serum bottles was flushed for 1 min with the same gas mixture also used for the respective cultivation. For growth of pre-cultures, 28 mM fructose was used as the carbon source with a N_2 atmosphere in the serum bottle. For autotrophic and mixotrophic experiments, a pre-mixed gas mixture of

80/20% (v/v) H_2/CO_2 (Air Liquide Austria GmbH, Schwechat, Austria) was used at a total pressure of 2.5 bar. The headspace was replaced daily with H_2/CO_2. During serum bottle cultivations, 2 mL samples were routinely withdrawn for OD_{600} determination and HPLC analysis.

Continuous cultivations were conducted either in a DASbox® Mini Bioreactor system (Eppendorf AG, Jülich, Germany) or in a DASGIP® Multibioreactor system (Eppendorf AG, Jülich, Germany). A filling volume of 200 mL and an agitation rate of 500 rpm were used for DASbox® cultivations and a filling volume of 1000 mL and an agitation rate of 400 rpm were used for cultivations with the DASGIP® system. For all cultivations, a temperature of 30 °C was used. The reaction volume was maintained at a constant volume using a dip tube and a peristaltic pump (Ismatec SA, Glattburg, Germany). An aeration rate of 0.25 vvm was applied. For the growth conditions H_2/CO_2, formate + H_2/CO_2 and formate + $H_2/CO/CO_2$, pre-mixed gas mixtures with CO (60:9.5:10.6:19% $H_2/CO/CO_2/N_2$) and without CO (60:9.5:29.6% $H_2/CO_2/N_2$) (Air Liquide Austria GmbH, Schwechat, Austria) were used. For growth on formate + fructose, nitrogen gas (purity in % >99.999) (Messer Austria GmbH, Gumpoldskirchen, Austria) was utilized. For growth on fructose alone, nitrogen and carbon dioxide (purity in % >99.995) (Air Liquide Austria GmbH, Schwechat, Austria) were mixed in a ratio of 80:20% N_2/CO_2 by the DASGIP® MX4/1 Gas Mixing Module (Eppendorf AG, Jülich, Germany).

The pH was maintained at 7.0 using 5 M KOH and 2 M phosphoric acid. The medium was sparged continuously with the indicated gases at a rate of 0.25 vvm. Offgas from the DASbox® Mini Bioreactor system was analyzed continuously with a gas chromatograph (Trace GC Ultra, Thermo Fisher Scientific, Waltham/MA, USA). Offgas from the DASGIP Multibioreactor system was analyzed continuously with a DASGIP® GA Exhaust Analyzing Module (Eppendorf AG, Jülich, Germany).

2.4. Biomass concentration determination

The cell dry weight was determined at steady state conditions as follows: 5 mL of freshly sampled culture broth were transferred into dried and pre-weighed glass tubes. The tubes were centrifuged for 10 min at 4 °C and 4,800 rpm (2,396 g), washed with 2.5 mL distilled water and centrifuged again. The samples were dried at 105 °C for 24 h, subsequently cooled in a desiccator for at least 1 h and finally weighed. For cultures grown on formate, a sample volume of 25 mL and a washing volume of 10 mL were used instead. Biomass determination was performed in triplicates. A correlation coefficient between OD_{600} and cell dry weight (biomass = 0.38*OD_{600}) was determined and used to estimate the biomass concentrations at all other points.

2.5. Bioreactor off-gas analysis

A Trace GC Ultra gas chromatograph (Thermo Fisher Scientific, Waltham/MA, USA) was used to analyze the reactor off-gas for H_2, CO, CO_2 and N_2. The gas chromatograph was equipped with a ShinCarbon ST 100/120 packed column (Restek Corporation, Bellefonte/PA, USA) and a thermal conductivity detector operated in constant temperature mode with 200 °C transfer temperature, 240 °C block temperature and 370 °C filament temperature. Argon 5.0 (Messer Austria GmbH, Gumpoldskirchen, Austria) was used as the carrier gas at a constant flow rate of 2.0 mL/min. Samples with a volume of 100 µL were injected with a split ratio of 20. After the injection, the oven temperature was kept constant at 30 °C for 6.5 min, then increased to a temperature of 250 °C with a 16 °C/min ramp and finally kept at 250 °C for 0.75 min. An electrical valve system allowed the automatic off-gas analysis of each of the four bioreactors of the DASbox system in 2 h intervals. The chromatograms were recorded and evaluated using Chromeleon 7.2.10 Chromatography Data System (Thermo Scientific, Waltham/MA, USA). Calibration was performed with premixed defined gas mixtures containing H_2, CO, CO_2 and N_2.

Off-gas analysis with the DASGIP® GA Exhaust Analyzing Module (Eppendorf AG, Jülich, Germany) was performed after calibrating the module with pressurized air and premixed calibration gas. The module was used to analyze the exhaust gas for CO_2.

2.6. Organic acid, sugar, and amino acid analysis

All organic acid, sugar and amino acid analysis were carried out with an Ultimate 3000 High Performance Liquid Chromatograph (HPLC) (Thermo Scientific, Waltham/MA, USA). Control, monitoring and evaluation of the analysis was performed with Chromeleon 7.2.6 Chromatography Data System (Thermo Fisher Scientific, Waltham/MA, USA).

Fructose, formate, and acetate quantification in sample supernatants were achieved with an Aminex HPX-87H column (300 × 7.8 mm, Bio Rad, Hercules/CA, USA). The mobile phase was 4 mM H_2SO_4, and the column was operated at a velocity of 0.6 mL/min, 60 °C for 30 min. Detection was performed with a refractive index (Refractomax 520, Thermo Fisher Scientific, Waltham/MA, USA) and a diode array detector (Ultimate 3000, Thermo Fisher Scientific, Waltham/MA, USA). Prior to analysis, 450 µL of culture supernatant were mixed with 50 µL of 40 mM H_2SO_4 and centrifuged for 5 min at 14,000 rpm (21,913 g) and 4 °C. 10 µL of this samples was injected for analysis (Erian et al., 2018). Standards at defined concentrations of fructose, formate, acetate, and ethanol were treated the same way.

Amino acids were analyzed with a reversed phase column (Agilent Eclipse AAA, 3 × 150 mm, 3.5 µm) with a guard column (Agilent Eclipse AAA, 4.6 × 12.5 mm, 5 µm) and a gradient of eluent (A) 40 mM NaH_2PO_4 monohydrate pH 7.8 and eluent (B) MeOH/ACN/MQ (45/45/10 (v/v/v)). At a flowrate of 1.2 mL/min and a column temperature of 40 °C, samples were analyzed with an injection volume of 10 µL. In-needle derivatization was performed with *ortho*-phtaldialdehyde (OPA) containing 1% 3-MPA and 9-Fluormethylencarbonylchlorid (FMOC). Samples and standards were spiked with norvaline and sarcosine as internal standards. Detection was carried out with a fluorescence detector (FLD-3400RS), detecting secondary amines and sarcosine at Ex 266 nm/Em 305 nm and primary amines and norvaline at Ex 340 nm/Em 450 nm (Hofer et al., 2018).

2.7. Rate calculations and elemental balancing

For determination of the volumetric acetate formation rate (r_{ace}) and biomass formation rate (r_X), the dilution rate D was multiplied with the average acetate and biomass concentration from at least two data points from steady state conditions. Volumetric fructose and formate consumption rates were calculated by multiplying the feed concentration with the dilution rate.

The calculation of volumetric gas uptake rates XUR [mmol L^{-1} h^{-1}] from GC data was performed as follows: the molar fraction of N_2, CO, CO_2 and H_2 were determined in the reactor exhaust gas. Mass balances were established assuming that no N_2 is consumed (NTR = 0). The reactor gas inflow rate was measured and balancing of N_2 allowed calculation of the reactor exhaust gas flow. All gas transfer rates [mmol L^{-1} h^{-1}] were calculated from the volumetric gas inflow rate q_{in} [L h^{-1}], the molar fraction of the respective gas in the inlet gas ($y_{x,in}$) and exhaust gas ($y_{x,out}$) and the calculated volumetric exhaust gas flow q_{out} [L h^{-1}] as follows:

$$XUR = \frac{q_{in} \cdot y_{x,in} - q_{out} \cdot y_{x,out}}{V_{molar} \cdot V_{reactor}}$$

where V_{molar} [L mol^{-1}] is the molar gas volume at 20 °C and 1.013 bar, and $V_{reactor}$ [L] is the filling volume of the bioreactor. No corrections for the dissolved gas in the harvest flow or the CO_2/HCO_3^- equilibrium were applied.

To perform elemental balancing, a carbon content of 45% (w/w) was used for *A. woodii* biomass (Godley et al., 1990). A degree of reduction (DoR) of 4.15 mol electrons per mol of carbon was assumed for biomass

(Rittmann et al., 2012). Yeast extract was neglected for the calculation of the C- and DoR-balance.

2.8. Transcriptome and proteome analysis

2.8.1. Sampling

After a culture reached steady state conditions, a 5 mL sample was withdrawn, divided into 1 mL aliquots, and centrifuged for 1 min at 11,000 g and −4 °C. After removing the supernatant, the pellet was snap-frozen in liquid nitrogen. The samples were stored at −80 °C until further processing.

2.8.2. RNA extraction and RNAseq

Cell pellets were resuspended in 1 ml Invitrogen TRIzol Reagent (ThermoFisher Scientific, Waltham/MA, USA) and lyzed using a Fast-Prep-24 (MP Biomedicals, Santa Ana/CA, USA) with 0.37 g of glass beads (0.1 mm diameter) at 6 m/s for 40 s. Samples were incubated at room temperature for 5 min and then centrifuged at 12,000 g for 5 min. 750 µl of the supernatant were mixed with 750 µl ethanol and RNA isolated using the Direct-zol RNA Miniprep Kit (Zymo Research, Irvine/CA, USA) according to the manufacturer's instructions. This Kit includes a DNAse treatment step. Integrity, Quality, and Quantity of the isolated RNA was checked on a 5200 Fragment Analyzer System (Agilent, Santa Clara/CA, USA) and a NanoDrop One UV–Vis Spectrophotometer (ThemoFisher Scientific, Waltham/, MA, USA).

Preparation of RNA libraries and Sequencing on an Illumina Next-Seq, v2.5, 1 × 75bp with a target of 5 million reads per sample was performed by Microsynth (Microsynth AG, Balgach, Switzerland). Transcriptomic data were uploaded to the SRA database (accession number PRJNA737050).

2.8.3. Transcriptome analysis

The obtained reads were inspected using FastQC v0.11.5, analyzed and quality trimmed using Trimmomatic (Bolger et al., 2014). A reference transcriptome was extracted from the reference genome of *A. woodii* DSM 1030 (Poehlein et al., 2012) and the corresponding gff file using gffread v0.12.7 (Pertea and Pertea, 2020). A salmon index was created by using salmon 1.4.0 (Patro et al., 2017) on the reference transcriptome and the samples were quantified, including the –gcBias flag to account for the effects of sample specific biases such as fragment-level GC bias. The quantification results were imported into the R environment and analyzed with the DESeq2 (Love et al., 2014) package and the packages tximport, ggplo2, vsn, pheatmap, RColorBrewer and limma (R Core Team, 2013; Soneson et al., 2016; Zhu et al., 2019).

2.8.4. Sample preparation for proteome analysis

For the proteomics analysis, samples were lysed in 100 µl of the lysis buffer (100 mM Tris pH 8.6, 1% sodium dodecyl-sulphate (SDS), 40 mM chloroacetamide and 10 mM (tris(2-carboxyethyl)phosphine) (TCEP)) followed by three cycles of sonication (15 s per cycle, 20% amplitude). Lysates were then spun down for 5 min at 14,000 *g* and 100 µg of protein (after protein estimation) were precipitated overnight using acetone. The following day, protein pellets were re-solubilized in 50 µl of 25% trifluoroethanol (TFE) in 100 mM Tris (pH = 8.6), after which solution was diluted to 10% TFE with 100 mM ammonium-bicarbonate and subjected to overnight digestion with trypsin (1:67 ratio protein to trypsin). Resulting peptide mixture was offline desalted, then chromatographically separated using an Ultimate 3000 RCS Nano Dionex system equipped with an Ionopticks Aurora Series UHPLC C18 column (250 mm × 75 µm, 1.6 µm) (Ionopticks, Australia). Solvent A was 0.1% formic acid in water and solvent B acetonitrile containing 0.1% formic acid. Total run per sample was 136.5 min with the following gradient: 0–5.5 min: 2% B; 5.5–65.5 min: 2–17% B; 65.5–95.5 min: 25–37% B, 105.5–115.5 min: 37–95% B, 115.5–125.5 min: 95% B; 125.5–126.5 min: 95-2% B; 126.5–136.5 min: 2% B at a flow rate of 400 nl/min and 50 °C. Peptides were measured on the timsTOF mass spectrometer (Bruker Daltonics, Germany) that was operated in positive mode with enabled trapped Ion Mobility Spectrometry (TIMS) at 100% duty cycle (100 ms cycle time). Scan mode was set to parallel accumulation–serial fragmentation (PASEF) for the scan range of 100–1700 m/z. Source capillary voltage was set to 1500 V and dry gas flow to 3 L/min at 180 °C.

2.8.5. Statistical analysis of proteome data

Raw data processing was carried out using MaxQuant (v1.6.17.0) (Cox and Mann, 2008; Tyanova et al., 2016a). Database matching was performed against a genome predicted publicly available *A. woodii* protein database (GCF_000247605.1_ASM24760v1; downloaded on February 24, 2021, 3546 entries). For peptide as well as protein matching, false discovery rate was set to 1%, minimum peptide length was set to six and up to two mis-cleavages were allowed. Oxidation of methionine was set as variable and carbamidomethylation as fixed modification. Match between run feature was enabled for the match window of 1 min and alignment window of 20 min.

Resulting table of protein "Intensities" was then imported to Perseus (v 1.6.14.0) (Tyanova et al., 2016b), where data was transformed, normalized (mean subtraction per column) and grouped. Matrix was then filtered to keep only those proteins with reported values in at least three replicates in at least one of the groups. Missing values were consequently imputed from normal distribution (downshift 1.8, width 3) and pairwise Student's t-tests were carried out between the groups with multi-testinging correction (permutation-based FDR <5%). All the raw proteomics data including the search parameters, database used as well as results output was deposited to the ProteomeXchange Consortium via the PRIDE partner repository (Perez-Riverol et al., 2019) with the dataset identifier PXD026569.

2.9. Metabolic modelling and FBA

A previously published *A. woodii* core model (Koch et al., 2019) with 118 reactions was used to perform flux balance analysis (FBA) and model intracellular fluxes. Energy conservation and redox balancing were considered by the model as previously described for *A. woodii* (Schuchmann and Müller, 2014). A biomass composition similar to *Clostridium autoethanogenum* was assumed (Valgepea et al., 2017). The *CellNetAnalyzer* toolbox (Klamt et al., 2007; von Kamp et al., 2017) was used for flux balance analysis (FBA). The experimentally determined specific rates for biomass formation, substrate uptake (formate, fructose, CO, CO_2, H_2) and metabolite formation were used to constrain the model. The determined rates beared redundancies with respect to carbon and redox balances in the metabolic model. Consequently, fluxes were corrected prior to the FBA calculations to obtain a consistent system. This was achieved by minimizing the relative changes in the measured rates needed to yield a consistent flux scenario ("Check feasibility" function in *CellNetAnalyzer*). The growth rate was kept constant under all conditions. As the objective function, the pseudo reaction that quantifies the non-growth associated ATP maintenance (NGAM) demand was maximized. Thereby, intracellular flux distributions and an upper bound of ATP available for NGAM processes could be described. To estimate variations in fluxes, flux variability analysis was performed with and without NGAM as the constraint.

3. Results and discussion

3.1. Chemostat cultivations to investigate physiology and systems level response of A. woodii

Even though formate has previously been used as a growth substrate for *A. woodii*, there is no quantitative data set describing the physiological behavior during growth on this one-carbon compound. Therefore, steady state cultivation data were obtained by establishing

chemostat cultivations of *A. woodii* at a dilution rate of 0.05 h^{-1}. This growth rate previously proved to be the half-maximum growth rate of *A. woodii* for the substrate conditions investigated here (Novak et al., 2021). A total of six different conditions were tested, including formate, H_2/CO_2, fructose, formate + H_2/CO_2, formate + H_2/CO_2/CO and formate + fructose (Table 1). For each steady state condition, the physiological behavior was investigated and complemented by transcriptomics (RNAseq) and proteomics analyses.

3.1.1. *A. woodii efficiently utilizes formate for growth and acetate production in chemostat cultures*

In a first step, we evaluated whether chemostat cultivations of *A. woodii* with formate as the sole carbon and energy source can be established. To that end, batch cultures were transferred to continuous mode by supplying a feed containing 100 mM formate at a rate of 0.05 h^{-1}. Indeed, cells completely consumed formate and stable steady state formation of biomass and acetate production was observed. However, carbon-limited cultures under these conditions showed extremely low biomass concentrations of 0.14 g L^{-1} (see Table 1). To evaluate whether the biomass concentration and the volumetric formate turnover could be boosted, the formate concentration in the feed was increased to 200 mM. As a result, the volumetric formate uptake rate roughly increased by 2-fold (Table 2) and formate was fully consumed. Although the formate concentration was doubled, steady state concentrations for biomass and acetate only increased by 57 and 71% to 0.22 g L^{-1} and 3.17 g L^{-1}, respectively (Table 1). A possible explanation is the yeast extract that was used in the same concentration for all cultivations. Yeast extract has been shown to increase biomass and acetate yields of *A. woodii* cultures (Tschech and Pfennig, 1984), thus leading to an overestimation of acetate yields on formate.

During growth on formate, 4 mol formate are required to form 1 mol acetate (Bertsch and Müller, 2015a). The remaining carbon is oxidized to 2 mol CO_2 to provide enough reduction power for carbon fixation in the WLP (Fig. 4). The reaction stoichiometry therefore shows a carbon efficiency of only 50%. Moreover, the ATP yield for stoichiometric formate conversion is only 0.3 ATP per mol acetate (Müller, 2019). Using 200 mM formate, near stoichiometric conversion of formate to acetate and CO_2 was observed. The yields for acetate and CO_2 were 0.26 mol mol^{-1} and 0.47 mol mol^{-1}, respectively. As the carbon and DoE balance were closed (Table 1), the influence of yeast extract seemed negligible for growth on 200 mM formate. The high amount of carbon liberated as CO_2 combined with a low ATP yield make formate a challenging anaerobic substrate and provide a possible explanation for the low biomass yields observed during growth of *A. woodii* on formate (Table 2).

Generally, specific rates can be used to extract information on the physiological behavior and boundaries of a microbial cell factory utilizing a given substrate. Additionally, sound physiological data are crucial to obtain useful results from metabolic modelling (section 3.3). Therefore, we next analyzed cell specific formate uptake and acetate formation rates of *A. woodii* during growth on formate. Despite the low biomass yields, a specific formate uptake rate of 47 mmol g^{-1} h^{-1} corresponding to ~1 g g^{-1} h^{-1} was observed for the 200 mM chemostat. Moreover, the specific production rate for acetate was ~12 mmol g^{-1} h^{-1}. Combined with the favorable acetate yields, these values indicate that *A. woodii* can convert formate to acetate at high rates and efficiency. *A. woodii* could therefore be an interesting organism for anaerobic formate-based bioproduction. Additionally, the data obtained here provide a reference data set under well-defined conditions which can be used for comparison of *A. woodii* physiology during formate utilization to other substrates.

3.1.2. *Quantitative comparison shows similarities of formate and autotrophic H_2/CO_2 utilization but not with heterotrophic fructose utilization*

To obtain a picture of the physiological behavior of *A. woodii* during growth on formate, H_2/CO_2 and fructose were studied as reference substrates for autotrophic and heterotrophic fermentation. Fermentation data for H_2/CO_2 (Kantzow et al., 2015; Novak et al., 2021) and fructose (Godley et al., 1990) have already been reported. However, to ensure comparability and to obtain samples for the transcriptomic and proteomic analyses we decided to generate the reference data for both substrates using the same cultivation conditions and media as for the formate cultivations. Changing only the respective carbon and energy sources, chemostat cultivations for both substrates were successfully established. Gas-limited cultures on H_2/CO_2 with a gas containing 60% H_2 and 9.5% CO_2 showed 4-fold higher biomass concentrations compared to the 200 mM formate culture (Table 1). This increase is also reflected in the biomass yield which was ~50% higher for H_2/CO_2 compared to formate (g mol^{-1} basis, Table 1). A higher biomass yield is

Table 1
Yield coefficients for biomass formation and acetate production during growth of *A. woodii* on single and mixed substrates. Mean values and standard deviations were calculated from biological triplicates.

Growth condition	Product concentration [g L^{-1}]		Acetate yields [mol mol^{-1} substrate]					Biomass yields [g mol^{-1} substrate]					Balances [%]	
	Acetate	Biomass	$Y_{Ace/For}$	$Y_{Ace/Fru}$	$Y_{Ace/CO2}$	$Y_{Ace/H2}$	$Y_{Ace/sumC}$	$Y_{X/For}$	$Y_{X/Fru}$	$Y_{X/CO2}$	$Y_{X/H2}$	$Y_{X/sumC}$	C	DoR
Formate (102 mM)	1.85 ± 0.07	0.135 ± 0.011	0.312 ± 0.011	–	–	–	0.312 ± 0.011	1.32 ± 0.11	–	–	–	1.32 ± 0.11	128 ± 7	154 ± 7
Formate (200 mM)	3.17 ± 0.05	0.22 ± 0.01	0.263 ± 0.005	–	–	–	0.263 ± 0.005	1.09 ± 0.03	–	–	–	1.09 ± 0.03	104 ± 1	113 ± 2
H_2:CO_2 (60:9.5)	15.3 ± 1.0	0.93 ± 0.10	–	–	0.449 ± 0.021	0.228 ± 0.012	0.449 ± 0.021	–	–	1.62 ± 0.14	0.82 ± 0.08	1.62 ± 0.14	96 ± 5	99 ± 5
Fructose (34.1 ± 0.5 mM)	4.77 ± 0.09	1.76 ± 0.07	–	2.33 ± 0.01	–	–	2.33 ± 0.01	–	51.5 ± 0.9	–	–	51.5 ± 0.9	108 ± 4	111 ± 2
Formate (100 mM) H_2:CO_2 (60:9.5)	16.3 ± 1.1	0.98 ± 0.06	2.71 ± 0.18	–	0.529 ± 0.015	0.244 ± 0.012	0.442 ± 0.011	9.8 ± 0.6	–	1.92 ± 0.12	0.89 ± 0.03	1.59 ± 0.07	94 ± 3	98 ± 1
Formate (100 mM) H_2:CO_2:CO (60:9.5:10.6)	16.2 ± 1.2	1.28 ± 0.01	2.70 ± 0.20	–	0.676 ± 0.003	0.285 ± 0.003	0.445 ± 0.001	12.8 ± 0.1	–	3.21 ± 0.24	1.35 ± 0.08	2.11 ± 0.15	97 ± 1	102 ± 1
Formate (202 ± 2 mM) Fructose (35.3 ± 1.1 mML)	7.88 ± 0.16	1.94 ± 0.03	0.649 ± 0.008	3.72 ± 0.04	–	–	0.553 ± 0.005	9.60 ± 0.05	55.0 ± 1.0	–	–	8.17 ± 0.02	106 ± 1	108 ± 1
H_2:CO_2:CO (60:9.5:10.6) [a]	17.8 ± 1.5	1.54 ± 0.12	–	–	0.43 ± 0.01	0.23 ± 0.01	–	–	–	–	–	–	93 ± 1	87 ± 1

[a] Data from (Novak et al., 2021).

Table 2
Volumetric and specific substrate uptake and acetate formation rates from *A. woodii* chemostat cultivations on single and mixed substrates. Mean values and standard deviations were calculated from biological triplicates. Specific rates are uptake rates (negative values for qCO_2 indicate production) for formate, fructose and H_2, CO_2 and CO, and production rates for acetate. Volumetricc rates are uptake rates (negative values for CO_2UR indicate production) for formate, fructose and H_2, CO_2 and CO, and production rates for acetate.

Growth condition	Dilution rate [h^{-1}]	Specific rates [mmol g^{-1} h^{-1}]						Volumetric rates [mmol L^{-1} h^{-1}]					
		qAce	qFor	qFru	qCO_2	qH_2	qCO	rAce	rFru	rFor	CO2UR	HUR	COUR
Formate (102 mM)	0.052 ± 0.002	11.89 ± 1.34	39.4 ± 4.8	–	−28.5 ± 1.3	−9.0 ± 2.7	–	1.59 ± 0.09	–	5.28 ± 0.21	−3.33 ± 0.26	−1.21 ± 0.38	–
Formate (200 mM)	0.051 ± 0.001	12.2 ± 0.3	47.0 ± 1.2	–	−22.5 ± 0.7	–	–	2.67 ± 0.06	–	10.3 ± 0.1	−4.92 ± 0.03	–	–
H_2:CO_2 (60:9.5)	0.054 ± 0.002	15.1 ± 1.1	–	–	33.8 ± 3.2	66.9 ± 7.5	–	14.0 ± 0.7	–	–	30.9 ± 0.9	60.9 ± 4.6	–
Fructose (34.1 ± 0.5 mM)	0.049 ± 0.001	2.20 ± 0.04	–	0.95 ± 0.02	0.07 ± 0.22	–	–	3.87 ± 0.06	1.66 ± 0.02	–	0.13 ± 0.40	–	–
Formate (100 mM) H_2:CO_2 (60:9.5)	0.055 ± 0.002	15.1 ± 0.3	5.6 ± 0.5	–	33.8 ± 3.2	66.9 ± 7.5	–	15.0 ± 0.9	–	5.47 ± 0.16	30.9 ± 0.9	60.8 ± 4.5	–
Formate (100 mM) H_2:CO_2:CO (60:9.5:10.6)	0.054 ± 0.002	11.6 ± 0.4	4.3 ± 0.2	–	17.2 ± 0.7	40.9 ± 2.0	4.6 ± 0.4	15.2 ± 0.6	–	5.51 ± 0.20	22.0 ± 1.0	52.3 ± 1.5	5.9 ± 0.6
Formate (202 ± 2 mM) Fructose (35.3 ± 1.1 mM)	0.050 ± 0.001	3.40 ± 0.04	5.24.0 ± 0.01	0.92 ± 0.02	−2.7 ± 0.1	–	–	6.60 ± 0.17	1.77 ± 0.06	10.2 ± 0.2	−5.17 ± 0.15	–	–
H_2:CO_2:CO (60:9.5:10.6) [a]	0.05	10.8 ± 0.4	–	–	17.1 ± 1.2	46.6 ± 2.2	8.7 ± 0.2	16.6 ± 0.7	–	–	26.2 ± 0.2	71.6 ± 2.3	13.4 ± 1.4

[a] Data from (Novak et al., 2021).

consistent with the higher carbon efficiency observed during growth on H_2/CO_2. Analogously to biomass, the acetate titer and yield were 4.8-fold and 70% higher for H_2/CO_2. However, the specific acetate productivity on formate was almost equal to the value of H_2/CO_2 (q_{Ace} 80% for formate compared to H_2/CO_2). Likewise, the specific uptake rates for all three carbon and energy sources were within the same range i.e., ~47 mmol g^{-1} h^{-1} for formate compared to ~34 mmol g^{-1} h^{-1} and 67 mmol g^{-1} h^{-1} for CO_2 and H_2, respectively. Hence, despite the drastic differences in titers and volumetric rates for the two conditions, a comparable physiological behavior could be observed. Regardless of the distinct differences to autotrophic growth, formate utilization of *A. woodii* via the WLP shares significant similarities with H_2/CO_2 utilization.

Next, fructose-grown chemostat cultures were compared to growth on formate. To ensure comparability, an equimolar amount of carbon (33.3 mM fructose) was used. Because fructose contains significantly more energy than formate (combustion energies of 2,930 kJ/mol and 245 kJ/mol, respectively), heterotrophic cultures have significantly higher ATP gains compared to formate cultures (see also 3.3.2). Consequently, the steady state biomass concentration of the fructose fermentation was 8-fold higher than for formate. As a result, the molar (g mol^{-1}) and C-molar (g C-mol^{-1}) biomass yields increased 50- and 8-fold, respectively. In contrast, the acetate titer was only increased by 50% (Table 1). The observed acetate yield of 2.33 mol mol^{-1} is in good agreement with previously reported values but it is only 78% of the theoretical maximum for homoacetogenic acetate production (Beck et al., 2019; Braun and Gottschalk, 1981; Wiechmann et al., 2020). Theoretically, acetogens could convert 1 mol of a hexose into 3 mol acetate by using CO_2 and reduction equivalents produced during sugar catabolism in the WLP for carbon fixation. However, the theoretical value does not consider that growth requires significant portions of cellular resources. As previously observed, heterotrophic cultures required CO_2 to fully consume fructose (Godley et al., 1990). The reason for this behavior is rooted in the function of the WLP as an electron sink. In the absence of sufficient amounts of CO_2, *A. woodii* cannot re-oxidize electron carriers.

A comparison of the specific rates showed that due to the high biomass concentrations of the heterotrophic cultures, substrate uptake rates for formate were ~50-fold higher compared to fructose. Similarly, the biomass specific acetate formation rate was 5.6-fold higher for formate. Combined, these observations could indicate that cells use high specific substrate turnover of low energy substrates to provide enough ATP for growth and maintenance of biomass, especially under anaerobic conditions (Rintala et al., 2008).

In conclusion, the physiological behavior of *A. woodii* during growth on formate and fructose differed significantly. These observations are in line with the different properties of the two substrates and the metabolic pathways involved in their utilization.

3.1.3. *Metabolic flexibility and robustness of A. woodii is revealed by efficient co-utilization formate with gaseous or heterotrophic substrates*

In a future bioeconomy, flexible substrate co-utilization is anticipated to become an important feature of microbial production hosts. Consequently, we investigated the ability of *A. woodii* to utilize formate together with H_2/CO_2 or fructose. Furthermore, a gas containing additional CO was tested for co-utilization with formate.

For gaseous co-substrates, the same gas-limited conditions as for the H_2/CO_2 condition described above were used to establish steady state continuous cultures. The liquid feed was supplied at D = 0.05 h^{-1} and initially contained formate (100 mM). Both conditions, formate + H_2/CO_2 and formate + H_2/CO_2/CO could successfully be established in carbon-limited chemostats. Generally, a stabilizing effect of formate on fermentation of gaseous substrates was noticed. In our previous study, autotrophic cultures were sensitive to perturbations (e.g. antifoam pump failure) that caused product titers and gas uptake rates to fluctuate and prohibited cultures to maintain steady state conditions (Novak et al., 2021).

A comparison to the 100 mM formate and the H_2/CO_2 culture showed that for formate + H_2/CO_2 the steady state acetate concentration was only 5% lower compared to the sum of acetate for the individual substrates (16.3 and 17.2 g L^{-1}, respectively) (Table 1). Similarly, the volumetric acetate productivity for formate + H_2/CO_2 was comparable to the sum of the induvial substrates. The biomass concentration for formate + H_2/CO_2 increased 5% compared to H_2/CO_2 but was 10% lower compared to the sum of the individual substrates. Compared to H_2/CO_2, formate addition to cultures did not affect the acetate yield (0.44 mol mol^{-1} for formate + H_2/CO_2, Table 1). This observation, however, might be a result of the relatively small contribution of formate to the final acetate titer as underlined by the specific substrate utilization rates. Although both cultures (formate and formate + H_2/

CO_2) were provided with the same volumetric formate feeding rate, the higher biomass concentration for formate + H_2/CO_2 decreased the specific formate uptake rate to only 14% of the value observed for unitrophic formate utilization (Table 2). Moreover, the presence of formate reduced the specific uptake rates for H_2 and CO_2 by 7 and 16%, respectively. These shifts in utilization of gaseous substrates indicate that formate partially replaced H_2 and CO_2 as energy and carbon sources under limiting chemostat conditions. Despite substrate co-utilization, the total specific acetate productivity for formate + H_2/CO_2 did not change compared to the H_2/CO_2 culture. This physiological behavior is in line with the observation that q_{Ace} was comparable when formate and H_2/CO_2 were used individually. Overall, the flexible adjustments of substrate utilization are quite remarkable given that co-utilization of formate and H_2/CO_2 requires the hydrogen-dependent CO_2 reductase (HDCR) of *A. woodii* to react to changing concentrations of educts and products of the reaction. For serum bottle cultures grown on increasing concentrations of formate and a H_2/CO_2 gas phase an initial lag phase was found. The length of the lag phase depended on the initial formate concentration (Fig. S1), indicating kinetic and thermodynamic regulation as the key determinant of flow at the HDCR. Regardless of potential initial inhibitions, all batch cultures eventually fully consumed formate and H_2/CO_2 from the gas phase and produced biomass and acetate.

Next, we expanded the investigation of co-utilization of formate and gaseous substrates to a gas stream which contained CO in addition to H_2/CO_2. In our previous study, we had shown that batch cultures containing formate + H_2/CO_2/CO first co-utilized formate and CO, and upon limitation of CO in the liquid culture, also H_2/CO_2 and CO. However, no information on the ability of *A. woodii* to co-utilize all four carbon and energy sources was gained. Chemostat cultures using 100 mM formate and H_2/CO_2/CO in the gas stream showed a 30% higher biomass concentration compared to formate + H_2/CO_2 (Table 1). CO is an intermediate of the WLP obtained by reducing CO_2 with the low potential reduction equivalent ferredoxin. When supplying limiting amounts of CO with CO_2/H_2, less ferredoxin is oxidized for CO_2 reduction (Novak et al., 2021). Hence, more ferredoxin can be allocated to the energy conserving reaction of the Rnf complex (section 3.3.2) (Schuchmann and Müller, 2014), improving overall bioenergetics, hence enabling an increase in biomass concentration (Bertsch and Müller, 2015a, 2015b; Novak et al., 2021).

In contrast to the biomass concentration, acetate titer, productivity and yield did not change for formate + H_2/CO_2/CO compared to formate + H_2/CO_2. Consequently, q_{Ace} decreased by 23% because of the higher biomass concentration (Table 2). A similar decrease was observed for the specific uptake rates for formate, H_2 and CO_2. For q_{H2} and q_{CO2}, the decrease was 34% and 40%, respectively. These changes indicate that in addition to the higher biomass concentration, cell specific rates were decreased by the presence of CO. Analogous to formate addition to H_2/CO_2 cultures, CO replaced H_2 and CO_2 as carbon and energy sources in the formate + H_2/CO_2/CO culture (see section 3.3 below for details on intracellular flux distributions). Collectively, *A. woodii* proved to be extremely flexible in utilizing up to four different carbon and energy sources simultaneously, including three gaseous substrates. Future work towards bioprocess development could further explore this important metabolic feature by varying formate and gas utilization and by expanding the system to other gas compositions. Combined, these measures will allow controlling specific uptake rates for individual substrates, which can be used as a strategy to control metabolism and intracellular fluxes (section 3.3.2 and 3.4).

Another substrate that could help to improve bioenergetics is the utilization of hexose sugars in combination with formate. *A. woodii* is known to efficiently utilize H_2/CO_2 and fructose but utilization together with formate has so far not been described. To that end, we aimed to establish continuous cultures fed with equimolar amounts of carbon from formate (200 mM = 200 mM carbon) and fructose (33.3 mM = 200 mM carbon). Carbon-limited steady states could be achieved which showed biomass and acetate concentrations of 1.9 and 7.9 g L^{-1}, respectively. These values are in both cases close to the sum of the cultures for formate and fructose utilization alone (Table 1). As formate was completely consumed, carbon catabolite repression (CCR) could not be observed even with the relatively high fructose concentrations. CCR was previously found to prevent co-consumption of methanol and glucose in *Eubacterium limosum* (Loubiere et al., 1992) and to cause poor H_2/CO_2 consumption by *Clostridium aceticum* (Braun and Gottschalk, 1981) and *Moorella thermoacetica* (Huang et al., 2012) in the presence of fructose or glucose, respectively. In contrast, in other acetogens including *Clostridium ljungdahlii*, gas consumption was not inhibited by fructose (Jones et al., 2016).

Furthermore, formate was able to replace the need for CO_2 to establish fructose-limited steady state conditions. As expected for formate utilization, co-utilization with fructose resulted in CO_2 production from formate (Table 2), indicating that formate served both as carbon and energy source in addition to fructose. The cell-specific fructose uptake rate was comparable for formate + fructose to fructose alone but due to the higher biomass concentration q_{For} was only 11% of the value for unitrophic formate utilization. Nevertheless, the presence of formate increased q_{Ace} by 50% compared to fructose utilization alone. This observation shows how co-utilization of a high and low energy substrate can improve physiological performance data beyond what is possible for unitrophic substrate utilization. While formate utilization improved cell-specific acetate productivity, fructose improved the overall bioenergetics. Consequently, addition of fructose or glucose could be used to improve the bioenergetics of formate-utilizing *A. woodii* in the future and enable shifting carbon flux away from acetate in metabolically engineered strains (section 3.4). In summary, the physiological data presented here demonstrate *A. woodii* as a robust host for formate-based bioconversion which can efficiently co-utilize autotrophic and heterotrophic carbon and energy sources in combination with formate.

3.2. A transcriptomic and proteomic analysis highlights substrate-specific regulation of pathways

The physiological study highlighted the ability of *A. woodii* to utilize different carbon and energy sources simultaneously. The individual substrates investigated are assimilated via separate pathways, provide different amounts of energy, and donate electrons with different potentials. However, biomass and acetate were the only products detected in the culture broth. The question arises how the cell flexibly adapts to various substrates while maintaining the same product spectrum.

Both formate and fructose were supplied to the culture by a liquid feed, possibly requiring the expression of genes for the uptake of these carbon sources from the medium. On the other hand, the one-carbon substrates formate, CO_2, and CO are all assimilated via the WLP, suggesting a similar overall metabolism and gene expression for autotrophic and formatotrophic growth. As formate is an intermediate of the methyl-branch of the WLP, simultaneous oxidation of formate to CO_2 and H_2 and activation of formate to formyl-THF might require fine-tuning of enzyme expression in the WLP. On top of that, co-utilization of formate with other substrates might require the activation of additional gene clusters e.g., for CO oxidation or fructose uptake. To thoroughly understand the utilization of different substrates and to examine the adaptation of the gene expression of *A. woodii*, we analyzed the transcriptome and proteome under different growth conditions.

RNA-seq allowed the detection of 3662 transcripts, covering the whole 3546 protein-coding ORF of the genome of *A. woodii*. Additionally, our investigation of the proteome is the first published LC-MS/MS-based proteome study for *A. woodii* and enabled the detection and quantification of 1881 polypeptides from all samples altogether. We performed a differential expression analysis of all six growth conditions using formate as reference condition (Fig. 1). The transcriptome of different growth conditions was investigated for similarities by identifying changes in the transcription of common genes.

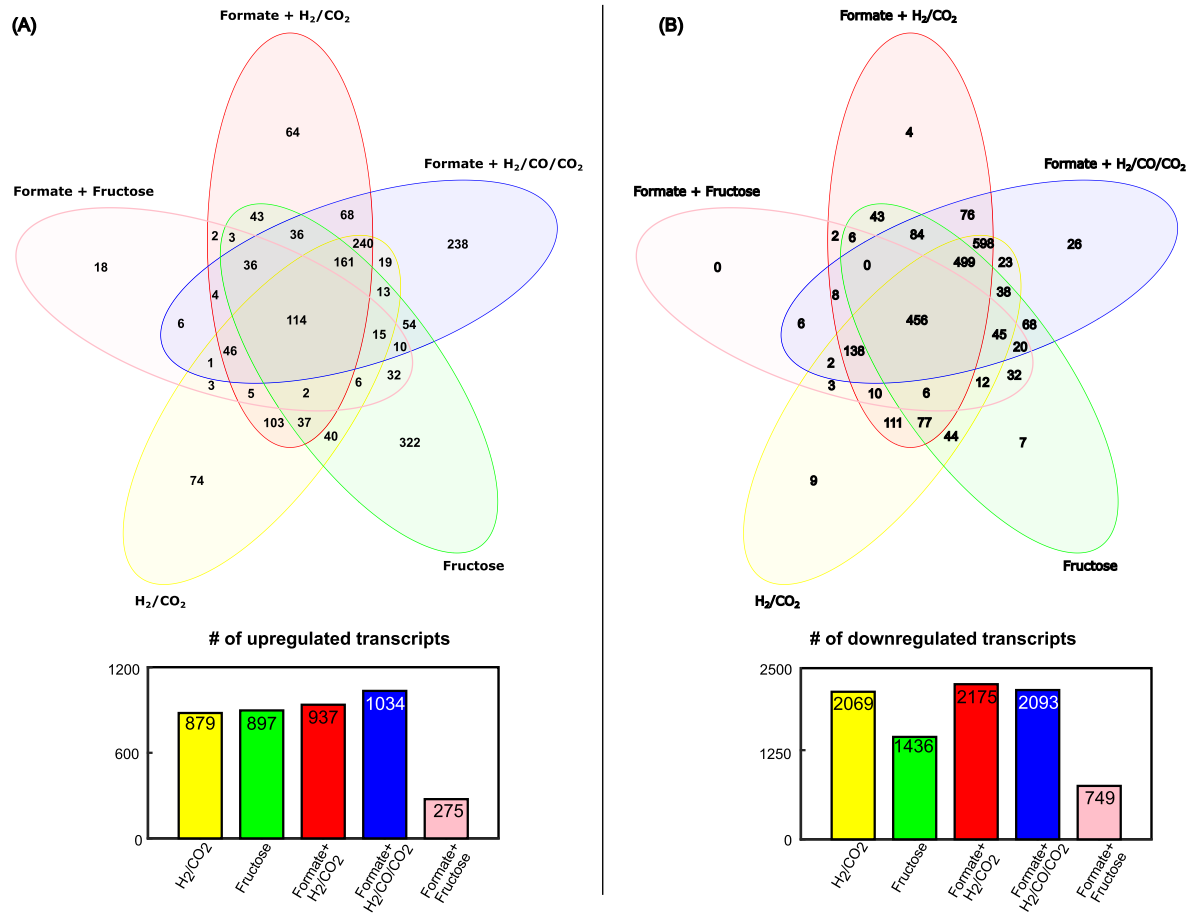

Fig. 1. Differential gene transcription analysis of *A. woodii* for growth on the six different substrate conditions tested. Figures indicate the number of differentially expressed genes as compared to growth on formate. (A) Number of upregulated genes; (B) number of downregulated genes.

456 genes were down-regulated and 114 genes were upregulated on a transcription level on all other growth conditions compared to formate, indicating an adaptation of the cell to the utilization of formate with high specific rates (47 mmol g^{-1} h^{-1}, section 3.1.1). For the other three growth conditions on one-carbon substrates (H_2/CO_2, formate + H_2/CO_2 and formate + $H_2/CO/CO_2$), 240 common genes were up-regulated and 598 common genes down-regulated as compared to growth on only formate. Under all three conditions, gaseous substrates were utilized and elevated acetate concentrations of ~15–17 g L^{-1} were reached (Table 1) which might trigger changes in the expression of common genes. With 264 and 329 exclusive changes in transcript levels, respectively, the growth conditions formate + $H_2/CO/CO_2$ and fructose indicated the most distinct adaptation to the respective substrates. In contrast, the growth on formate + fructose revealed only 275 up-regulated genes and 749 down-regulated genes as compared to growth on formate, indicating a similar transcriptome for these conditions.

This first differential analysis of the transcriptome suggests that *A. woodii* adapts to the supply of different substrates on a global level. In a previous proteome analysis of *A. woodii,* enzymes linked to glycolysis and the WLP were found to be expressed differently on fructose and H_2/CO_2 (Poehlein et al., 2012). In contrast, previous -omics studies of the acetogens *Clostridium ljungdahlii* and *Clostridium autoethanogenum* suggested a stable expression of genes under various substrate uptake and product formation rates, indicating a robust expression as the basis for metabolic flexibility of acetogens (Richter et al., 2016; Valgepea et al., 2017).

We next aimed to understand central adaptations in the expression of genes and proteins that are involved in acetate and biomass formation. To that end, we focused on the two central pathways that lead to acetyl-CoA synthesis (WLP, glycolysis + pyruvate decarboxylation), on enzymes involved in the supply of reduced reduction equivalents (electron bifurcating hydrogenase HydABCD, HDCR, Rnf complex) and on proteins that catalyze the conservation of energy (ATPase, Pyruvate kinase, Phosphoglycerate kinase).

3.2.1. *The WLP is highly expressed during growth on one-carbon substrates*

The WLP is responsible for the assimilation of the one-carbon substrates formate, CO_2, and CO. All one-carbon substrates were found to be taken up by *A. woodii* with high specific rates (section 3.1.2), indicating a highly active WLP.

Indeed, gene clusters of the methyl-branch of the WLP and the carbon monoxide dehydrogenase/acetyl-CoA synthetase (CODH/ACS) (Poehlein et al., 2012) were among the 20 genes that showed the highest intermediate normalized mean read count across all growth conditions (Fig. S2). A third highly transcribed gene cluster is the electron-bifurcating hydrogenase which is responsible for the oxidation of H_2 and supplying the WLP with reduced ferredoxin (Fd^{2-}) and NADH. To compare the expression of the WLP between growth conditions and to highlight up- and downregulation, differential transcriptome and proteome analyses were performed (Fig. 2).

Comparing the gene expression during growth on formate and H_2/CO_2 revealed comparable levels of expression for most genes of the WLP. However, the monofunctional CODH CooS and the neighboring iron-sulfur protein (Awo_c19060) and the CODH/Acetyl-CoA synthase β subunit AcsB2 were upregulated under autotrophic growth, both on a transcriptome and proteome level. This upregulation of genes of the WLP may be linked to the higher specific acetate formation rate (25% increased) during autotrophic growth compared to formatotrophic

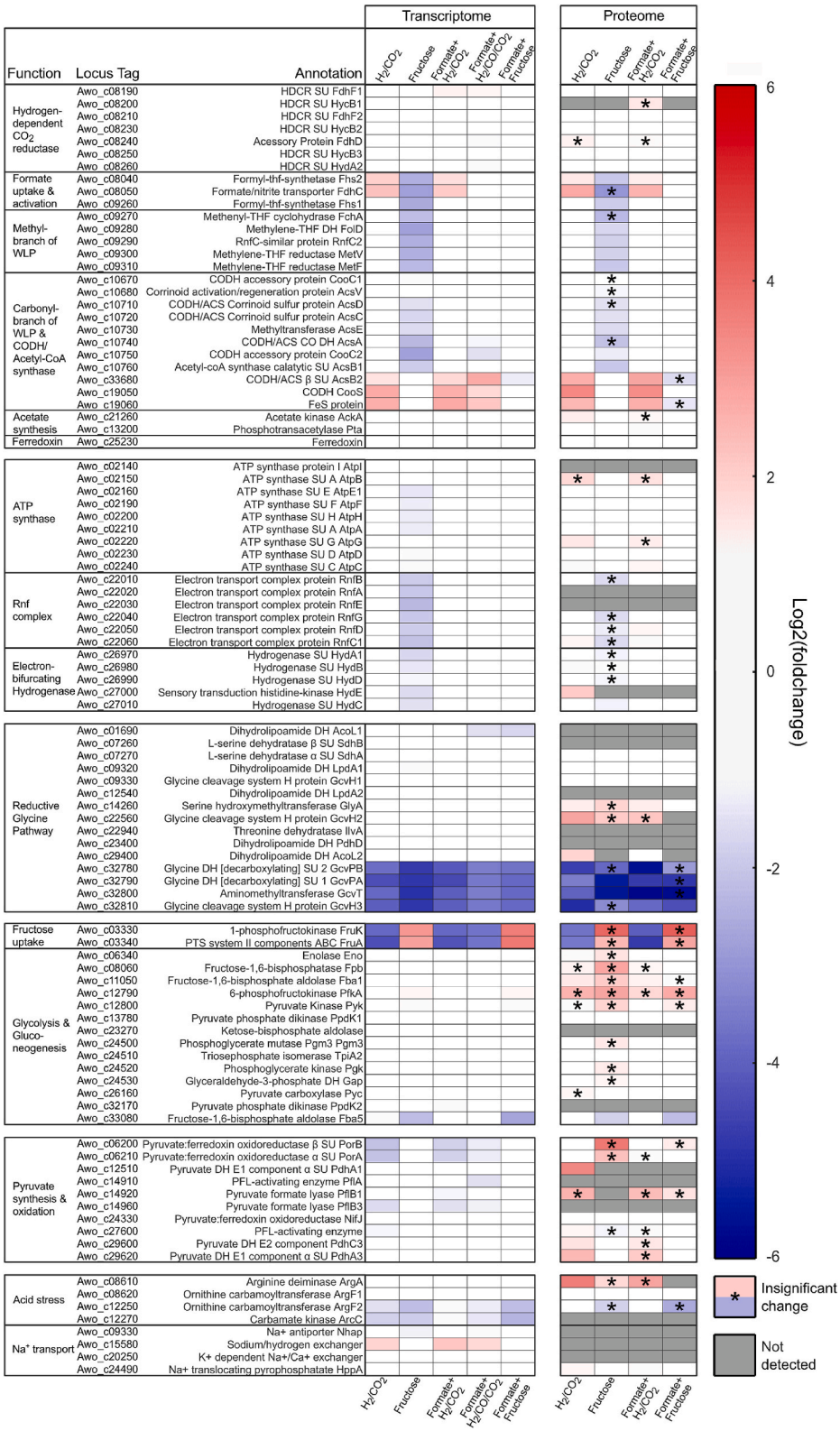

Fig. 2. Differential transcriptomic and proteomic analysis for growth of *A. woodii* on single and mixed substrates. Formate was chosen as the reference growth condition. SU = subunit, DH = dehydrogenase, PFL = pyruvate formate lyase.

growth (Table 2). A comparison of the proteome also revealed 2- to 4-fold higher levels for the ATPase subunits C and G, the electron transport complex protein RnfC1 and the Hydrogenase associated proteins B and E for autotrophic growth.

Heterotrophic growth on fructose showed several adaptations of the expression of genes of the WLP compared to growth on formate: transcript and protein levels of genes involved in the methyl-branch and genes of the CODH/Acetyl-CoA synthase were found in significantly lower levels (3- to 7-fold lower transcript levels, 3- to 5-fold lower protein levels) (Fig. 2). Transcriptome analysis additionally revealed 2-

to 5-fold lower transcript levels of several ATPase, Rnf complex and Hydrogenase subunit genes. The low specific acetate formation during growth on fructose requires only a small contribution of the WLP to acetate formation (section 3.3). As the WLP genes are among the highest transcribed genes in *A. woodii*, cutting back their expression potentially allows the cell to save energy. In contrast, the HDCR was not regulated on a transcript and protein level. H_2 serves as a substrate of the HDCR and needs to be provided via oxidation of NADH and Fd^{2-} during growth on fructose (Wiechmann et al., 2020). Providing a high HDCR activity might therefore be necessary to capture intracellular H_2 and funnel it towards the WLP.

The comparison of gene expression for growth on formate and formate + H_2/CO_2 revealed changes similar to the comparison of gene expression for growth on formate and autotrophic growth on H_2/CO_2. In detail, the same genes of the WLP showed higher transcript and protein levels (Fig. 2). The similar specific H_2 uptake rates for autotrophic growth and growth on formate + H_2/CO_2 (Table 2) may dictate the regulation of the WLP. Moreover, the co-utilization of formate + $H_2/CO/CO_2$ revealed similar transcriptional changes of the WLP genes as observed for the other growth conditions with gaseous substrates with a few notable exceptions. Compared to growth on H_2/CO_2 and formate + H_2/CO_2, formate + $H_2/CO/CO_2$ showed a weaker up-regulation of the monofunctional CODH CooS, a lower transcript number of the CODH accessory protein Cooc2 and a higher transcript level of the CODH/ACS β subunit AcsB2. These findings indicate an adaptation to the external supply of CO. By reducing the level of transcripts for CODH functions, an unnecessary assignment of Fd^{2-} for the reduction of CO_2 to CO might be avoided (section 3.3.1).

Compared to growth on formate, higher transcript and protein levels of the formyl-THF-synthetase Fhs2 and the putative formate transporter FdhC were found for H_2/CO_2 and formate + H_2/CO_2 but not for formate + $H_2/CO/CO_2$. In addition to a similar expression of Fhs2 and FdhC, the conditions formate and formate + $H_2/CO/CO_2$ share a specific acetate formation rate of ~12 mmol g^{-1} h^{-1} which is 20% lower than for growth on H_2/CO_2 and formate + H_2/CO_2 (Table 2). Potentially, a faster formation of acetate causes the intracellular pH to drop. A lowered intracellular pH at a constant external pH impairs the diffusive uptake of formic acid from the medium which is supposedly facilitated by FdhC (Moon et al., 2021). At low intracellular pH values, stronger expression of FdhC might therefore enable faster equilibration of internal and external formate pools. In contrast, stronger expression of Fhs2 might allow faster formate activation to keep the intracellular formate pool low and to avoid formate efflux into the medium.

A. woodii grown on formate + fructose showed almost no adaptations of the expression of the WLP compared to formate-grown cultures. This finding agrees well with the observation that there were few overall changes in the transcriptome between the two growth conditions (Fig. 1). A high level of WLP enzymes might be required to fully convert the additionally supplied formate.

The expression of the WLP adapts to the supplied carbon sources despite carrying the strongest transcribed genes throughout all growth conditions on single carbon sources. Surprisingly, lower transcript and protein levels of AcsB2 and CooS were found for growth on formate compared to growth on gaseous substrates, indicating a potentially lower activity of the acetyl-CoA generating step of the WLP. However, the expression of genes of the methyl-branch was not changed during growth on formate. The methyl-branch of the WLP can also fuel the reductive glycine pathway (rGLY), another carbon fixation pathway recently described in the acetogen *Clostridium drakei* (Song et al., 2020). Therefore, we next examined the expression level of genes of the rGLY.

3.2.2. The glycine cleavage system is upregulated during growth on formate

Compared to cultures grown under all other conditions, formate-grown cultures showed a strong expression of the genes GcvPA, GcvPB, GcvT and GcvH3 with an 11- to 32-fold increase on a transcript level and a 7- to 55-fold increase on a protein level. These genes are neighboring in the genome of *A. woodii* (see Fig. 3) and are part of the glycine cleavage system (GCS) that allows both glycine synthesis from one-carbon substrates and the degradation of glycine. The GCS forms a functional subunit of the reductive glycine pathway (rGLY) (Bar-Even et al., 2013).

An upregulation of the GCS could indicate a potential flux of one carbon metabolites to glycine. Nevertheless, the remaining genes of the rGLY that allow pyruvate synthesis from glycine via serine (Fig. 3) were not upregulated during growth on formate (Fig. 2). It is therefore hard to estimate the actual activity of the rGLY. To investigate the function of the GCS, we examined if glycine was accumulating in the medium or taken up. During growth on formate and fructose the small amounts of glycine that were provided with the feed (via yeast extract) were almost completely consumed (Table 3). The highest specific uptake rate was determined for growth on formate, being 8-fold higher than for growth on fructose. The transcript changes observed for the GCS genes *gcvPA, gcvPB, gcvT* and *gcvH3* were drastically higher than in a recent study that compared the transcriptome of *A. woodii* batch cultivations on formate, fructose and H_2/CO_2 (Moon et al., 2021). Our carbon-limited continuous cultivation on formate with a high ratio of glycine to biomass potentially triggered the increased expression of the GCS to enable the uptake of glycine as an additional carbon and energy source. For growth on fructose, a bigger share of glycine might have been directly incorporated into biomass, rendering an upregulation of the GCS obsolete.

Despite the role of the GCS in glycine degradation, *A. woodii* could theoretically use the rGLY for assimilation of single carbon sources. The acetogen *C. drakei* was shown to possess all genes of the rGLY as well. For *C. drakei*, metabolic modelling suggested an almost negligible flux through the rGLY and CO_2 fixation mainly via the WLP and the glycine synthase-reductase pathway (GSRP) (Song et al., 2020). *A. woodii* is lacking a glycine synthase-reductase and can therefore only fix CO_2 via the rGLY and the WLP. To further analyze the importance of glycine-forming pathways in the one carbon assimilation of *A. woodii* and other acetogens, further investigations are necessary.

3.2.3. Pyruvate synthesis is not regulated on a gene expression level

During growth on one-carbon substrates such as formate, CO and CO_2, the synthesis of pyruvate is based on the carboxylation of acetyl-CoA. Pyruvate is an important metabolite that links CO_2 fixation to major biomass-forming reactions. The genome of *A. woodii* encodes two pyruvate:ferredoxin oxidoreductases (PFOR), three pyruvate formate lyases (PFL), and three pyruvate dehydrogenases (PDH) that could be responsible for the carboxylation of acetyl-CoA. The Fd^{2-}-consuming PFOR reaction is considered the active pyruvate synthesis route in acetogens (Furdui and Ragsdale, 2000). However, the PFL reaction would allow acetogens to synthesize pyruvate from formate, thereby saving valuable Fd^{2-} for other reactions. To investigate the role of different pyruvate-forming enzymes under different growth conditions, we examined their expression level on a transcript and protein level.

We calculated the transcript level for each gene by multipying the intermediate normalized mean read count with the read length (75 bp) and dividing it by the length of the respective gene. The PFOR gene *nifJ* was identified as the highest transcribed gene for pyruvate synthesis: the transcript level of 255 for *nifJ* was ~5-fold higher than the transcript levels of the highest transcribed PDH genes *pdhC3, pdhB3* and *pdhA3,* ~7-fold higher than the PFOR subunit genes *porA* and *porB,* and ~90-fold higher than the highest transcribed PFL gene *pflB3*. NifJ was also measured in all proteome samples and showed the highest intensity of all pyruvate-forming enzymes.

A comparison of transcript and protein levels revealed stable expression of NifJ under all growth conditions. Stable and strong expression of *nifJ* indicates that pyruvate synthesis via acetyl-CoA might indeed rely on the PFOR reaction. To verify the importance of NifJ or other pathways for pyruvate synthesis in more detail, activities from PFOR, PDH and PFL enzymes in crude extracts could be analyzed for different conditions using *in vitro* assays. Additionally, the generation of

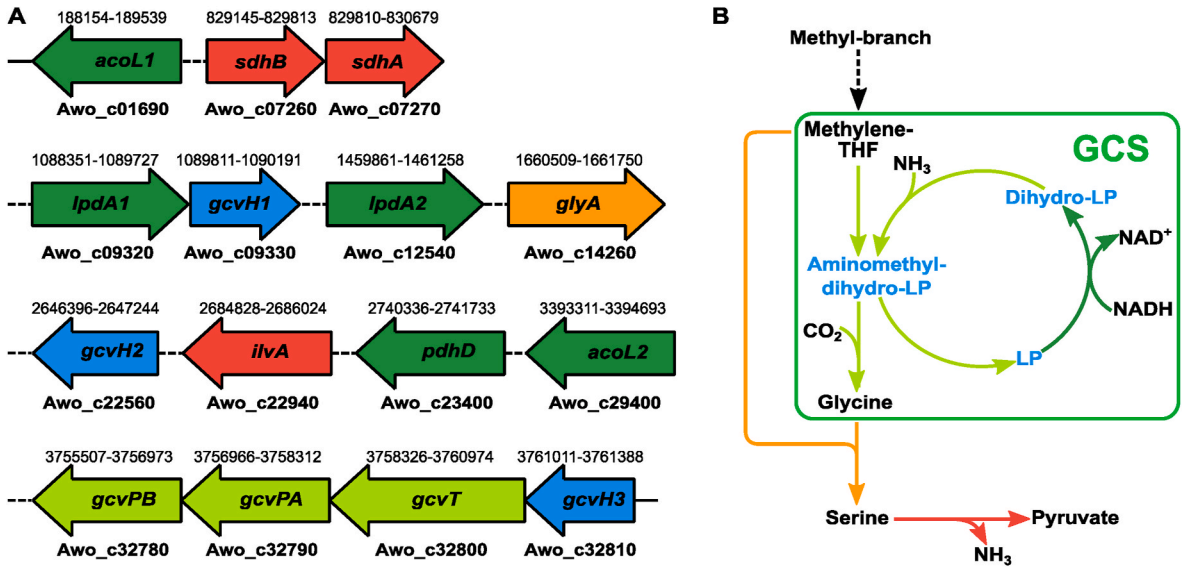

Fig. 3. Arrangement and function of the genes associated to the reductive glycine pathway of *A. woodii*. A: Genomic organization of rGLY genes. acoL1, acoL2, lpdA1, lpdA2 and pdhD: Dihydrolipoamide dehydrogenase; sdhB and sdhA: L-serine dehydratase subunits; gcvH1, gcvH2 and gcvH3: Glycine cleavage system H-Protein; glyA: Serine hydroxymethyltransferase; ilvA: Threonine dehydratase; gcvPB and gcvPA: Glycine dehydrogenase subunits; gcvT: Aminomethyltransferase; B: Metabolic map of the rGLY. LP: Lipoprotein.

Table 3
Glycine uptake rates for A. woodii chemostat cultivations on single substrates. A glycine concentration of 307 ± 12 μM was determined for the feed. r_{Gly}, volumetric glycine uptake rate, g_{Gly}, specific glycine uptake rate. Dilution rates and biomass concentrations from Tables 1 and 2

Condition	Formate	H_2/CO_2	Fructose
r_{Gly} [μmol L^{-1} h^{-1}]	14.1	4.0	14.7
q_{Gly} [μmol g^{-1} h^{-1}]	67	4.3	8.5
Relative glycine consumption [%]	89	24	96

a *nifJ* deletion mutant might be interesting for future studies as it would enable pyruvate formation via the PFL reaction. The PFL route via formate and acetyl-CoA was already shown to be feasible *in vivo* in anaerobically-grown *E. coli* (Zelcbuch et al., 2016).

3.2.4. Fructose supply activates uptake via the phosphotransferase system

In contrast to growth on one-carbon substrates, the direct supply of fructose allows the synthesis of pyruvate via glycolysis. Fructose utilization is initiated by substrate uptake via the phosphotransferase system (PTS). During growth on fructose and formate + fructose, a 2.5- to 4-fold increase in the transcript levels of *fruA* and *fruK* was noted compared to growth on formate (Fig. 2). Therefore, the expression of the fructose uptake system seems to be linked to the presence of fructose in the growth medium.

3.2.5. Site product formation is regulated during growth on different carbon sources

A. woodii is equipped with the genetic information to produce several fermentation products including lactate and ethanol. The genes for lactate utilization and potential lactate formation are organized in the operon lctCDEF. In our study, the highest transcript levels of the lctCDEF operon were found in formate-grown cells with 13- to 20-fold higher transcription compared to growth on fructose (Fig. S3). A down-regulation of this operon was previously described for growth on fructose, H_2/CO_2, methanol, and ethylene glycol. The operon was shown to be activated by the presence of D- and L-lactate, leading to a ~300-fold increase in the transcription level (Schoelmerich et al., 2018). Hence, the operon was not fully activated for growth on formate and the low transcription underlines why no lactate was formed under any of the growth conditions.

Ethanol formation from fructose has been described for phosphate-limited cultures of *A. woodii* (Buschhorn et al., 1989). Current studies highlighted the importance of the bi-functional alcohol dehydrogenase AdhE for ethanol formation and consumption of *A. woodii* (Trifunović et al., 2020). Interestingly, ~4-fold higher *adhE* transcript levels were found in fructose-grown cells as compared to formate-grown cells. The AdhE protein was detected in all analyzed fructose samples (Fig. S3). Ethanol formation from acetyl-CoA could serve as an alternative electron sink to the WLP. Interestingly, ethanol was neither detected in the culture supernatant of our study nor in studies where the re-oxidation of reduction equivalents via the WLP was blocked (Godley et al., 1990; Wiechmann et al., 2020). Further research is needed to understand the relevance of AdhE during growth of *A. woodii* on fructose.

3.2.6. A single ferredoxin is dominantly expressed

Ferredoxin serves as a carrier for electrons with a low reduction potential. Fd^{2-} is critical for the reduction of CO_2 in the carbonyl-branch of the WLP but also plays a crucial role in building up the sodium gradient at the Rnf complex which drives ATP synthesis. The genome of *A. woodii* encodes eleven potential ferredoxins. Among those, Awo_c25230 is transcribed with the highest intermediate normalized mean read count and without changes between different growth conditions (Fig. 2). Awo_c25230 was also detected in all proteome measurements, underlining the abundance and importance of this ferredoxin.

3.3. Metabolic modelling highlights major differences of intracellular flux levels and directionality

The data obtained from chemostat cultivations were used to perform flux balance analysis with the stoichiometric core model of *A. woodii*. Metabolic modelling enabled us to investigate which pathways are involved in the utilization and co-utilization of substrates, to highlight reactions that build the fundament for the high metabolic flexibility of *A. woodii,* and to access the turnover of reduction equivalents and the available energy. Maximizing non-growth associated ATP maintenance (NGAM) was used as an objective function. To check flux variations, flux variability analysis (FVA) was additionally performed (File S2).

Modelling the growth of *A. woodii* on formate suggested a high flux of

13 mmol L^{-1} h^{-1} through the WLP (Fig. 4). Formate was partly degraded by the HDCR to supply the cell with CO_2 and H_2. 94% of the acetyl-CoA formed was converted to acetate to gain ATP via substrate level phosphorylation. The remaining share of acetyl-CoA was fueling anabolic reactions of the cell. During growth on formate, the overall supply of electrons was insufficient to reduce all CO_2 formed from formate degradation, leading to a net release of CO_2. When the uptake of glycine from the medium was neglected, the flux from methylene-THF to glycine via the GCS was 100-fold smaller than the flux through the WLP, indicating a minor role of the GCS as carbon fixation pathway under these conditions. Including a glycine uptake rate of 67 μmol g^{-1} h^{-1} (Table 3) as an additional constraint for FBA did not increase degradation of glycine

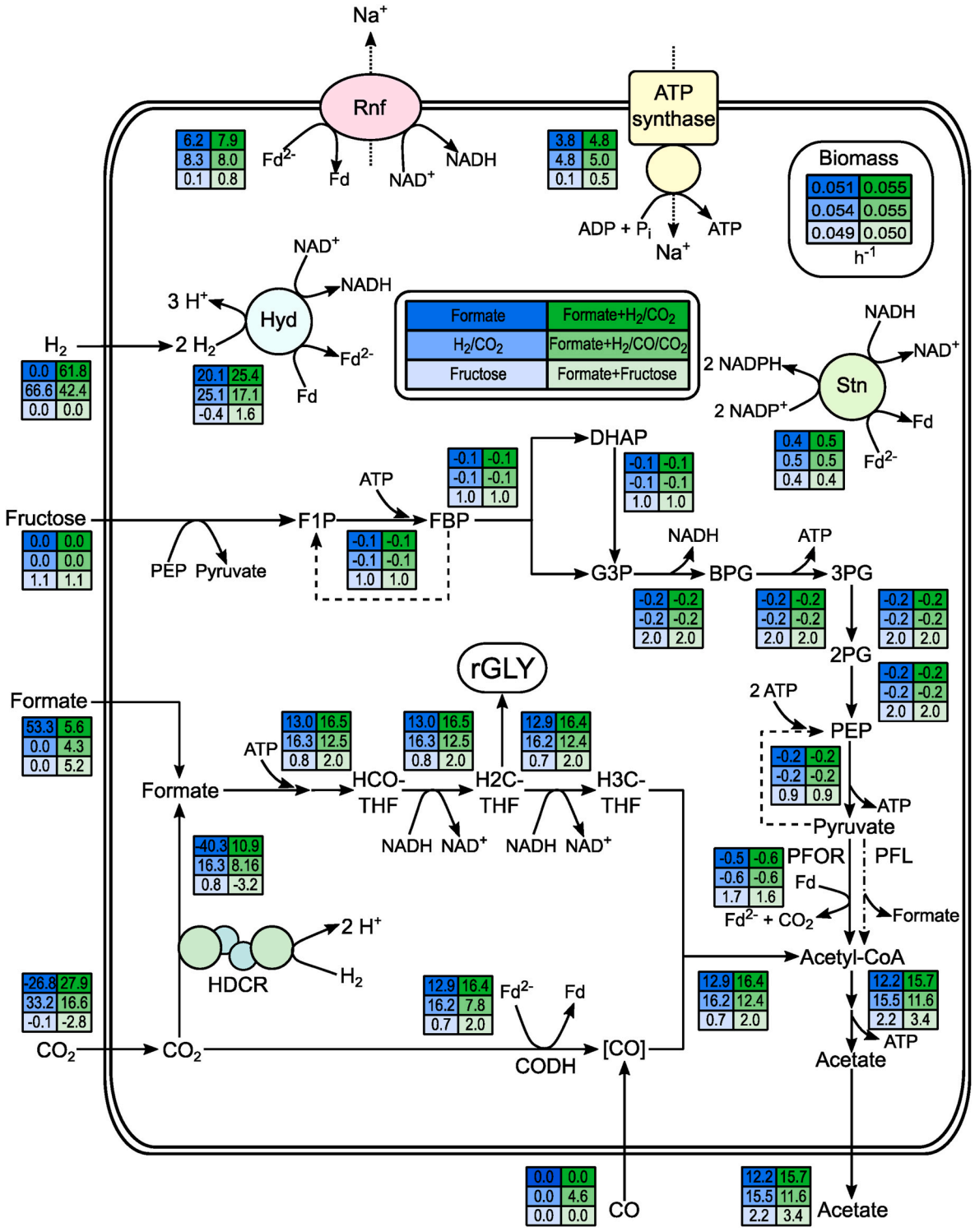

Fig. 4. Metabolic flux map of *A. woodii* for growth on different substrates. Boxed values show flux levels in mmol g^{-1} h^{-1} for six different growth conditions. rGLY = reductive glycine pathway, Rnf = Rnf complex, Hyd = electron-bifurcating hydrogenase, Stn = *Sporomusa* type Nfn (Kremp et al., 2020), HDCR = hydrogen-dependent carbon dioxide reductase, PFOR = pyruvate:ferredoxin oxidoreductase, PFL = Pyruvate formate lyase, F1P = fructose-1-phosphate, FBP = fructose bisphosphate, DHAP = dihydroxyacetone phosphate, G3P = glyceraldehyde-3-phosphate, BPG = bis-phosphoglycerate, 3 PG = 3-phosphoglycerate, 2 PG = 2-phosphoglycerate, PEP = phosphoenolpyruvate.

via the GCS (data not shown), which is in stark contrast to the distinct upregulation of GCS gene expression (section 3.2.2). However, the glycine uptake rate was ~800-fold lower compared to the formate uptake rate, providing a potential explanation for the negligible influence on intracellular flux distributions.

Growth on H_2/CO_2 led to a 25% higher flux through the WLP as compared to growth on formate, agreeing well with the higher expression of WLP genes (section 3.2.1). Formate was formed from H_2 and CO_2 by the HDCR instead of being lysed. Apart from the HDCR reaction, the metabolic fluxes were similar to formatotrophic growth.

Heterotrophic growth on fructose varied significantly from the formatotrophic and autotrophic condition. The degradation of fructose via glycolysis provided energy via substrate level phosphorylation and central carbon metabolites for anabolic reactions, making costly gluconeogenesis obsolete. The direction of the hydrogenase reaction was inverted to form H_2 from NADH and Fd^{2-}. The flux through the WLP was only 66% of the initial fructose uptake rate, underlining the role of glycolysis as the central energy-providing pathway. Despite a lower expression of WLP gene clusters (section 3.2.1), the WLP allowed full reoxidation of reduction equivalents obtained from fructose degradation.

The growth on formate + H_2/CO_2 revealed flexible adaptation of fluxes to the available substrates. External formate fueled the internal metabolite pool and reduced the reaction rate of the HDCR by 33% compared to growth on H_2/CO_2. However, the overall flux to acetyl-CoA remained unchanged. For growth on formate + $H_2/CO/CO_2$, formate and CO fueled the carbonyl-branch and the methyl-branch of the WLP.

Growth of *A. woodii* on formate + fructose represented a metabolic mixture of the growth on the isolated carbon sources. Fructose was degraded via glycolysis to provide energy and metabolites for the anabolism. Simultaneously, formate was used as a substrate of the WLP, providing additional energy. The flux through the WLP to acetyl-CoA was ~280% of the flux during growth on fructose, thereby contributing significantly to acetate production and energy generation. This increased flux was supported by a stronger expression of WLP genes as compared to growth on fructose (section 3.2.1). However, the activity of the WLP was still 6.5-fold lower than for growth on formate. When co-utilizing formate and fructose, 39% of formate was activated by the formyl-THF-synthetase while the remaining part was converted to CO_2 and H_2. Hence, the reduction equivalents obtained from glycolysis allowed to utilize more formate in the methyl-branch as compared to growth on formate. Formate was shown before to serve as an electron acceptor in the methyl-branch of the WLP (Wolin et al., 2003; Wiechmann et al., 2020). However, the CO_2 released from formate and fructose degradation equaled the amount that was released for growth on formate (section 3.1.3).

Comparing modelling results for different growth conditions highlights reactions and pathway functionalities and explains the metabolic flexibility of *A. woodii*: the direction of the hydrogenase reaction is adapted to allow either oxidation of H_2 for the supply of reduction equivalents or generation of H_2 for formate synthesis via the HDCR. Excess formate is lysed by the HDCR to release H_2 to provide additional reduction power. While the expression level of the HDCR is not adapted (section 3.2.1), the fluxes from H_2/CO_2 to formate vary greatly in direction and overall level for the different growth conditions. The stable expression of the HDCR might enable complete and fast utilization of the electron donors formate and H_2.

3.3.1. *A. woodii utilizes the WLP for energy conservation and as a redox sink*

Generally, the WLP serves as an electron sink (Schuchmann and Müller, 2014). In *A. woodii*, electrons are provided by oxidation of H_2, fructose, CO or formate-derived H_2. We investigated the provision and consumption of reduction equivalents by eight key reactions of the central carbon metabolism to underline differences in their fate and the contribution of the WLP to their reoxidation (Fig. 5).

During growth on formate and H_2/CO_2, all Fd^{2-} is supplied by the oxidation of H_2 through the hydrogenase HydABCD. 75% of NADH is obtained by H_2 oxidation and the remaining part by oxidation of Fd^{2-}. Nearly all NADH and the remaining Fd^{2-} are consumed in the WLP while the gluconeogenetic reactions (PFOR and G3P DH) and NADPH

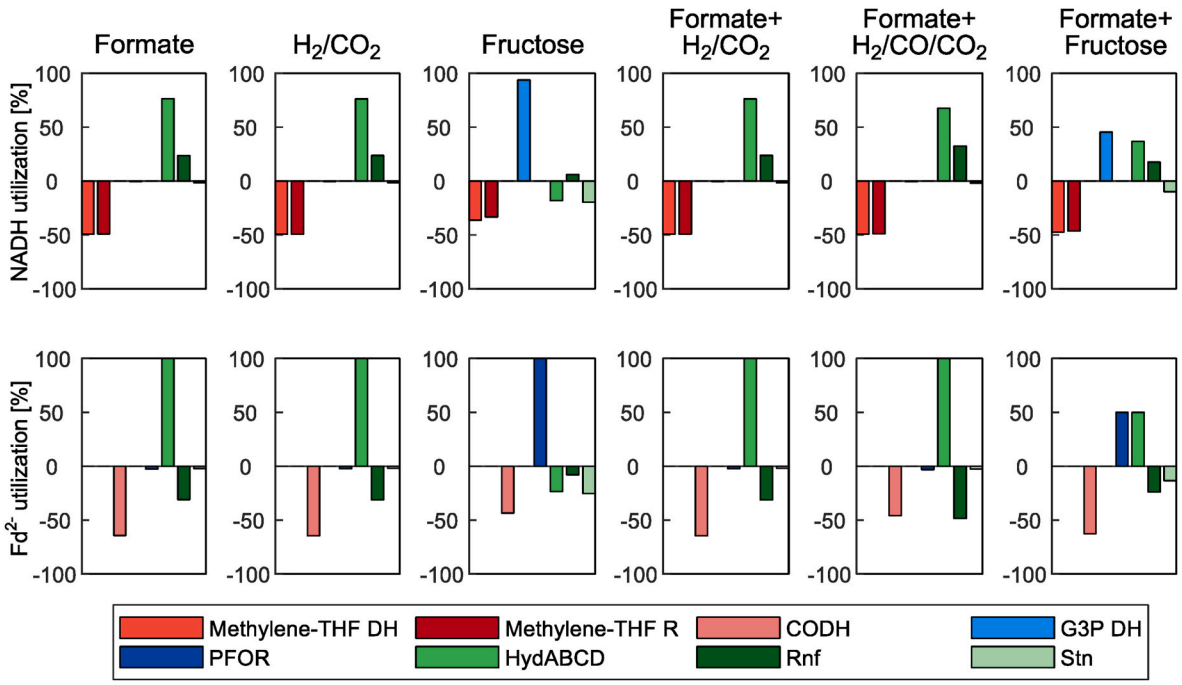

Fig. 5. Relative contribution of central redox reactions to the NADH and Fd^{2-} pool under different substrate conditions. Negative rates indicate oxidation of the respective reduction equivalent, positive rates reduction. Reaction rates were normalized by the total rate of reduction of each reduction equivalent by all eight considered reactions. DH = dehydrogenase, R = reductase, G3P = 3-phosphoglycerate, PFOR = pyruvate:ferredoxin oxidoreductase, HydABCD = electron bifurcating hydrogenase, Rnf = Rnf complex, Stn = *Sporomusa* type Nfn. The rates for the generation and consumption of NADH and Fd^{2-} were derived from the metabolic modelling results (Fig. 4).

forming reaction (Stn) contribute to a negligible amount. The overall contribution of reactions to the supply and oxidation of reduction equivalents is identical for formatotrophic growth and autotrophic growth on H_2/CO_2.

In contrast, PFOR is the sole source of Fd^{2-} during heterotrophic growth on fructose. The electron-bifurcating hydrogenase operates in reverse direction and consumes NADH and Fd^{2-} to supply H_2 for formate formation by the HDCR. Only 6% of NADH are generated from Fd^{2-} via the Rnf complex, correlating with the lower expression of Rnf complex genes (section 3.2.1). Compared to growth on formate, a bigger share of NADH (19%) and Fd^{2-} (25%) is consumed via Stn, guiding reduction power towards NADPH-consuming anabolic reactions (Kremp et al., 2020). Nevertheless, the WLP still functions as an electron sink during growth on fructose. Due to the minor contribution of the Rnf complex in redox balancing, the function of the WLP and Rnf complex in energy conservation becomes subordinate.

Co-utilization of formate + H_2/CO_2 relies on the oxidation of H_2 to provide electrons, similar to the respective unitrophic growth conditions, resulting in an identical share of redox reactions in the conversion of reduction equivalents. When formate + $H_2/CO/CO_2$ are co-utilized, Fd^{2-} is also exclusively generated from oxidation of H_2. However, less Fd^{2-} is consumed by the CODH and 48% of Fd^{2-} is oxidized via the Rnf complex.

During growth on formate + fructose, electrons are equally provided from formate-derived H_2 and glycolytic redox reactions. Half of the Fd^{2-} is provided by the electron-bifurcating hydrogenase and the other half by the PFOR. 18% of NADH are generated by the reaction of the Rnf complex, indicating a stronger role of the WLP in energy conservation compared to growth on fructose. A notable share of electrons is transferred to NADPH via Stn to fuel anabolic reactions.

A. woodii can flexibly adapt to the electrons supplied by substrate oxidation. While re-oxidation of reduction equivalents by the WLP is crucial during heterotrophic growth, energy conservation via the Rnf complex was found to play only a minor role. All electrons and carbon sources are used to produce acetyl-CoA via the glycolysis and the WLP, yielding acetate as the only product in addition to biomass.

Establishing *A. woodii* as a platform organism for formate-based bioproduction requires an extension of the product spectrum to industrially relevant bulk and commodity chemicals. To understand the formation of acetate as the sole product and to determine potential limitations for the synthesis of other products, we examined the ATP availability of *A. woodii* for growth on different substrates.

3.3.2. Co-utilization of substrates allows modulation of ATP availability

The synthesis of ATP from acetyl-CoA plays an important role in the energy household of *A. woodii*: during autotrophic and formatotrophic growth. During growth on fructose, acetate formation from pyruvate-derived acetyl-CoA enables synthesis of additional ATP. Acetyl-CoA is also an intermediary metabolite for the synthesis of industrially relevant products (Vees et al., 2020). However, withdrawing acetyl-CoA for the synthesis of metabolites other than acetate is only possible if net energy conservation of the cell is ensured. Consequently, product yields are constrained by ATP availability (Bertsch and Müller, 2015b).

To investigate the available energy of *A. woodii*, the ATP gain per acetate was calculated (Table 4). The metabolic model of *A. woodii* allowed consideration of energetic costs for gluconeogenesis which are necessary to evaluate growth-coupled production of metabolites. A second approach to access the ATP availability of the cell is to determe the non-growth associated ATP maintenance (NGAM) which reflects the surplus ATP that cannot be associated to growth.

During growth on formate, the lowest ATP/acetate ratio of 0.2 was determined, being 91% of the value for growth on H_2/CO_2 (Table 5). Both for formatotrophic and autotrophic growth, a high specific acetate formation rate was required to supply the cell with sufficient energy. Consequently, little energy could be invested in energy-negative production pathways. The NGAM value for growth on formate was 56% lower than for autotrophic growth on H_2/CO_2. The lower ATP maintenance costs might be linked to the low acetate concentration of 3.1 g L^{-1} for the formatotrophic culture as compared to the high acetate concentration of 15.3 g L^{-1} for the autotrophic cultivation on H_2/CO_2. We found an inhibitory effect of high acetate concentrations on growth of *A. woodii* in our previous study (Novak et al., 2021) and a link between ATP maintenance costs and acetate concentrations has already been postulated for other acetogens (Valgepea et al., 2017). Integrating glycine uptake into the FBA for growth on formate increased the NGAM value by ~5%, indicating that glycine uptake may have increased ATP availability when formate was the carbon source.

Growth of *A. woodii* on fructose allowed the highest ATP generation per formed acetate, being 5.2-fold higher than for growth on formate. The NGAM value for growth on fructose was 2.5-fold higher than for growth on formate and was comparable to the value for autotrophic growth on H_2/CO_2 (Table 4). As the acetate concentration of 4.8 g L^{-1} for heterotrophic growth was comparable to the concentration for growth on formate, product inhibition is unlikely to be responsible for the increased ATP maintenance costs. Analyzing samples from fructose-limited chemostat cultivations under the microscope showed *A. woodii* cells to be noticeably motile in contrast to cells from formatotrophic and autotrophic cultures. Thus, the higher ATP availability during growth on fructose might have enabled energy investment into inefficient cellular functions such as movement, thereby increasing maintenance costs.

For co-utilization of formate + H_2/CO_2, the same ATP gain per acetate was determined as for autotrophic growth on H_2/CO_2. The NGAM values for both conditions were also comparable. As the supply route of reduction equivalents is the same (section 3.3.1), assuming a similar energy state of the cell seems plausible. For growth on formate + $H_2/CO_2/CO$, a 41% higher ATP gain was observed as compared to formate + H_2/CO_2. Improved bioenergetics through supply of CO is in line with previous reports for *A. woodii* and other acetogens (Hermann et al., 2020; Novak et al., 2021). Supplying CO directly to the carbonyl-branch of the WLP enabled lower specific flux through the WLP while maintaining the same specific flux through the Rnf complex (section 3.3.1).

When growing on formate + fructose, a 3.8-fold higher ATP gain per acetate was observed compared to growth on formate. By providing fructose in a molar concentration six times lower compared to formate, the energetic availability of the cell could be drastically increased. The computed NGAM value was 2.9-fold higher than for growth on formate, indicating that the addition of fructose increased the amount of ATP wasted. Indeed, cells grown on formate + fructose were also motile when inspected under the microscope.

In conclusion, the mixing of low energy substrates, e.g., formate and H_2, with energy-rich substrates, e.g., CO and fructose, allows improving the bioenergetics of *A. woodii*. This additional energy could ultimately

Table 4
ATP yields per formed acetate and non-growth associated ATP maintenance (NGAM) for growth of *A. woodii* on different substrate mixtures. For calculation of the yields, the reactions of the following enzymes were considered: Formyl-THF synthetase, ATPase, acetate kinase, PTS fructose, 6-phosphofructokinase, phosphoglycerate kinase, pyruvate kinase.

Condition	Formate	H_2/CO_2	Fructose	Formate + H_2/CO_2	Formate + $H_2/CO/CO_2$	Formate + Fructose
ATP Yield (mol ATP/mol Acetate)	0.20	0.22	1.04	0.22	0.31	0.75
Non-growth associated ATP maintenance (NGAM)	0.6473[a]	1.4549	1.6445	1.4460	1.6225	1.8528

[a] The NGAM value was 0.681 mmol g^{-1} h^{-1} when a glycine uptake rate of 0.067 mmol g^{-1} h^{-1} was used as an additional constraint in FBA.

Table 5
Comparison of the energetic efficiency of different acetogens and microorganisms during growth and product formation on one carbon substrates and sugar substrates. Energetic efficiency was calculated according to (Claassens et al., 2019). rGLY (eng.) refers to engineered, synthetic formatotrophy.

Organism	Substrate	Active assimilation pathway	Product(s)	Energetic efficiency [%]	Reference
A. woodii	Formate	WLP	Acetate	84.2	Tschech and Pfennig (1984)
A. woodii DSM1030		WLP	Acetate	93.7	This study
A. woodii DSM1030		WLP	Acetate	80.7	Moon et al. (2021)
E. coli		rGLY (eng.)	Biomass	18.8	Kim et al. (2020)
C. necator		rGLY (eng.)	Biomass	21.2	Claassens et al. (2020)
C. necator		Calvin cycle	Biomass	23.7	Claassens et al. (2020)
Pseudomonas 1		Serine cycle	Biomass	52.2	Goldberg et al. (1976)
Methylotroph strain M2		Serine cycle	Biomass	60.4	Kelly et al. (1994)
A. woodii DSM1030	Formate + H_2/CO_2	WLP	Acetate	75.2	This study
A. woodii DSM1030	Formate + H_2/CO_2/CO	WLP	Acetate	78.2	This study
A. woodii DSM1030	H_2/CO_2	WLP	Acetate	76.3	This study
C. ljungdahlii		WLP	Acetate, Ethanol, 2,3BDO (check)	80.8	Hermann et al. (2020)
C. autoethanogenum	$H_2/CO/CO_2$	WLP	Acetate, Ethanol, 2,3BDO	79.6	Valgepea et al. (2017)
C. ljungdahlii		WLP	Acetate, Ethanol, 2,3BDO	76.3	Hermann et al. (2020)
A. woodii DSM1030		WLP	Acetate	75.1	Novak et al. (2021)
C. ljungdahlii	CO	WLP	Acetate, Ethanol, 2,3BDO (check)	72.1	Hermann et al. (2020)
C. autoethanogenum		WLP	Acetate, Ethanol, 2,3BDO	69.6	Valgepea et al. (2018)
P. pastoris PC4002	Methanol	DHA cycle	Biomass	36.1	Shay et al. (1987)
P. pastoris CBS 704		DHA cycle	Biomass	36.9	Hazeu and Donker (1983)
Pseudomonas 1		Serine cycle	Biomass	34.1	Goldberg et al. (1976)
Pseudomonas C		Serine cycle	Biomass	48.7	Battat et al. (1974)
B. methanolicus MGA3		RuMP cycle	Biomass	43.3	Schendel et al. (1990)
B. methanolicus MGA3		RuMP cycle	Biomass	45.1	Pluschkell and Flickinger (2002)
E. coli		rGLY	Biomass	11.8	Kim et al. (2020)
A. woodii DSM1030+		WLP	Acetate	82.7	Tschech and Pfennig (1984)
Acetobacterium sp.+		WLP	Acetate	87.0	Bainotti et al. (1998)
Acetobacterium sp.	Methanol + Formate	WLP	Biomass	74.4	Bainotti and Nishio (2000)
C. acetobutylicum CAB1060	Glucose	–	Butanol, Ethanol	65.4	Nguyen et al. (2018)
S. cerevisiae		–	Ethanol, Glycerol	81.6	Nissen et al. (1997)
A. woodii DSM1030	Fructose	WLP	Acetate	65.0	Godley et al. (1990)
A. woodii DSM1030		WLP	Acetate	69.2	This study
A. woodii DSM1030	Formate + Fructose	WLP	Acetate	74.3	This study

be used to synthesize relevant bulk chemicals from sustainable carbon and energy sources such as H_2, formate, CO, and CO_2. Genetic tools for the plasmid-based overexpression of pathways and for the deletion of genes in *A. woodii* are available (Beck et al., 2019; Hoffmeister et al., 2016; Wiechmann et al., 2020), enabling to broaden the product spectrum in the future. As *A. woodii* naturally directs all excess carbon and reduction equivalents towards the formation of acetate, additional genetic modifications might be needed to improve heterologous product synthesis.

3.4. Formate-based bioproduction achieves excellent energy efficiencies

One-carbon sources such as CO_2, CO, formate and methanol are considered as promising platform feedstocks of the future bioeconomy (Bar-Even et al., 2013; Claassens et al., 2019; Cotton et al., 2020). Table 5 shows the energetic efficiencies obtained for *A. woodii* and different substrates used in this study and compares them to values reported for acetogens and other common microbial hosts. Overall, acetogens show superior energetic efficiency on all substrates analyzed, with the highest values for one carbon substrates. Compared to gaseous substrates, formate as a miscible one carbon substrate showed even higher energetic efficiencies. The high efficiency make formate a promising substrate for bioproduction of chemicals and fuels. However, acetogens such as *A. woodii* and *E. limosum* (Litty and Müller, 2021) form acetate as the exclusive product during growth on formate. Metabolic engineering of *A. woodii* might allow to implement strategies for production of other metabolites. Production of ethanol and lactate from the substrates considered in this study were analyzed using flux balance analysis (Table 6). To that end, NGAM values and specific substrate uptake rates from experimental results (Fig. 4 and Table 4) were used as model inputs together with a specific growth rate of 0.02 h^{-1} and maximizing the ethanol or lactate yield was used as objective function. Metabolic modelling showed that by smart co-feeding of substrates flexible production scenarios for formate upgrading with high energy efficiencies can be devised. Supplementation of relatively minor quantities of CO and fructose increases the energy availability (section 3.3.2), and thus enables exclusive formation of ethanol or lactate without co-production of acetate. Co-utilization of H_2 allows complete fixation of CO_2, improving the carbon efficiency of the process or even facilitating net CO_2 uptake. The superior energy efficiency and straight forward substrate co-utilization make *A. woodii* an excellent candidate for formate-based bioproduction.

4. Conclusion

The quantitative physiological, transcriptomic, proteomic, and computational analysis of this study revealed *A. woodii* metabolism to be highly flexible in terms of substrate co-utilization. The -omics analysis together with metabolic modelling provided insights into the adaptations of acetogen metabolism to utilization of different substrates. Utilization of formate, autotrophic and heterotrophic substrates was characterized by high energetic efficiencies, a crucial aspect for economic viability of bioprocesses for chemicals and fuels production from one carbon substrates. *In silico* analysis underlined the potential of substrate co-utilization for improving the bioenergetics which could facilitate the implementation of metabolic engineering strategies for formate-based production of ethanol and lactate. Collectively, the results of this study highlight *A. woodii* as a promising host for bioprocesses rooted in sustainable substrates.

Conflict of interests

The authors declare no competing interests.

Table 6
In silico predictions of the efficiency of formate-based bioproduction of ethanol and lactate with *A. woodii*. Reaction stoichiometries were obtained from FBA simulations (q_{For} = 50 mmol g^{-1} h^{-1}, μ = 0.02 h^{-1}, experimentally determined NGAM values for the individual conditions used from Table 4). AdhE = bifunctional alcohol dehydrogenase, Aor = aldehyde oxidoreductase, Ldh = lactate dehydrogenase, Co-Ldh = electron-confurcating lactate dehydrogenase.

Product	Pathway	Co-substrate (s)	Reaction Stoichiometry (normalized)	Energetic efficiency [%]
Ethanol	AdhE	none	100 Formate = 14.2 Acetate + 6.6 Ethanol + 56.8 CO_2	87.1
	Aor		100 Formate = 16.1 Ethanol + 66.2 CO_2	89.4
	AdhE	Fructose	100 Formate + 1.5 Fructose = 19.2 Ethanol + 69.3 CO_2	90.0
	AdhE	H_2/CO_2	100 Formate + 66 CO_2 + 332.4 H_2 = 32.1 Acetate + 50.1 Ethanol	86.6
	AdhE	H_2/CO_2/CO	100 Formate + 66 CO_2 + 9.2 CO + 361.1 H_2 = 27.0 Acetate + 45.8 Ethanol	70.9
	AdhE	CO	100 Formate + 24.7 CO = 20.2 Ethanol + 82.6 CO_2	88.1
	AdhE	H_2/CO	100 Formate + 38.8 CO + 276.1 H_2 = 68.6 Ethanol	87.3
Lactate	Ldh	none	100 Formate = 19.4 Acetate + 3.1 Lactate + 50.1 CO_2	86.1
	Co-Ldh		100 Formate = 14.2 Acetate + 6.6 Lactate + 50.1 CO_2	87.1
	Ldh	Fructose	100 Formate + 8.6 Fructose = 33.2 Lactate + 50.1 CO_2	90.8
	Co-Ldh		100 Formate + 2.3 Fructose = 20.7 Lactate + 50.1 CO_2	90.1
	Ldh	H_2/CO_2	100 Formate + 66 CO_2 + 232.2 H_2 = 56.7 Acetate + 17 Lactate	85.4
	Co-Ldh		100 Formate + 66 CO_2 + 232.2 H_2 = 54.8 Lactate	87.8
	Ldh	H_2/CO_2/CO	100 Formate + 66 CO_2 + 9.2 CO + 221.4 H_2 = 45.9 Acetate + 27.2 Lactate	91.0
	Co-Ldh		100 Formate + 66 CO_2 + 9.2 CO + 221.4 H_2 = 57.8 Lactate	93.0
	Ldh	CO	100 Formate + 90.6 CO = 31.2 Lactate + 95.4 CO_2	86.7
	Co-Ldh		100 Formate + 24.7 CO = 20.2 Lactate + 62.4 CO_2	88.1
	Ldh	H_2/CO	100 Formate + 403.1 CO + 503.3 H_2 = 167.1 Lactate	86.0
	Co-Ldh		100 Formate + 31.6 CO + 131.8 H_2 = 43.3 Lactate	87.5

CRediT authorship contribution statement

Christian Simon Neuendorf: Investigation, Writing – original draft, Visualization. **Gabriel A. Vignolle:** Formal analysis. **Christian Derntl:** Investigation, Formal analysis. **Tamara Tomin:** Investigation, Formal analysis. **Katharina Novak:** Investigation. **Robert L. Mach:** Resources. **Ruth Birner-Grünberger:** Resources, Methodology. **Stefan Pflügl:** Conceptualization, Writing – original draft, Resources, Supervision, Project administration, Funding acquisition.

Acknowledgements

The authors are indebted to Samuele Verra for excellent technical assistance with the amino acid analysis. voestalpine Stahl GmbH, OMV Downstream GmbH and Austrian Airlines AG are gratefully acknowledged for financial support and the Austrian Research Promotion Agency (FFG) for funding. The authors acknowledge TU Wien Bibliothek for financial support through its Open Access Funding Program.

Appendix A. Supplementary data

Supplementary data to this article can be found online at https://doi.org/10.1016/j.ymben.2021.09.004.

Funding

CN (#874503), KN (#858702), and SP (#858702, #874503) received funding from the Austrian Research Promotion Agency (FFG). TT and RBG received funding from the Austrian Science fund (FWF) (Doctoral school "DK Metabolic and Cardiovascular disease" (W1226) and SFB "Lipid hydrolysis" (F73)), Medical University of Graz and TU Wien.

References

Arora, N.K., Mishra, I., 2019. United Nations sustainable development goals 2030 and environmental sustainability: race against time. Environmental Sustainability 2, 339–342. https://doi.org/10.1007/s42398-019-00092-y.

Bainotti, A.E., Nishio, N., 2000. Growth kinetics of Acetobacterium sp. on methanol-formate in continuous culture. J. Appl. Microbiol. 88, 191–201. https://doi.org/10.1046/j.1365-2672.2000.00854.x.

Bainotti, A.E., Yamaguchi, K., Nakashimada, Y., Nishio, N., 1998. Kinetics and energetics of Acetobacterium sp. in chemostat culture on methanol-CO2. J. Ferment. Bioeng. 85, 223–229. https://doi.org/10.1016/S0922-338X(97)86772-4.

Balch, W.E., Schoberth, S., Tanner, R.S., Wolfe, R.S., 1977. Acetobacterium, a new Genus of hydrogen-oxidizing, carbon dioxide-reducing, anaerobic bacteria. Int. J. Syst. Bacteriol. 27, 355–361. https://doi.org/10.1099/00207713-27-4-355.

Bar-Even, A., Noor, E., Flamholz, A., Milo, R., 2013. Design and analysis of metabolic pathways supporting formatotrophic growth for electricity-dependent cultivation of microbes. Biochim. Biophys. Acta Bioenerg. 1827, 1039–1047. https://doi.org/10.1016/j.bbabio.2012.10.013.

Battat, E., Goldberg, I., Mateles, R.I., 1974. Growth of Pseudomonas C on C1 compounds: continuous culture. Appl. Microbiol. 28, 6.

Beck, M.H., Flaiz, M., Bengelsdorf, F.R., Dürre, P., 2019. Induced heterologous expression of the arginine deiminase pathway promotes growth advantages in the strict anaerobe Acetobacterium woodii. Appl. Microbiol. Biotechnol. https://doi.org/10.1007/s00253-019-10248-9.

Bertsch, J., Müller, V., 2015a. CO metabolism in the acetogen Acetobacterium woodii. Appl. Environ. Microbiol. 81, 5949–5956. https://doi.org/10.1128/AEM.01772-15.

Bertsch, J., Müller, V., 2015b. Bioenergetic constraints for conversion of syngas to biofuels in acetogenic bacteria. Biotechnol. Biofuels 8, 210. https://doi.org/10.1186/s13068-015-0393-x.

Blank, L.M., Narancic, T., Mampel, J., Tiso, T., O'Connor, K., 2020. Biotechnological upcycling of plastic waste and other non-conventional feedstocks in a circular economy. Curr. Opin. Biotechnol. 62, 212–219. https://doi.org/10.1016/j.copbio.2019.11.011.

Bolger, A.M., Lohse, M., Usadel, B., 2014. Trimmomatic: a flexible trimmer for Illumina sequence data. Bioinformatics 30, 2114–2120. https://doi.org/10.1093/bioinformatics/btu170.

Boone, D.R., Johnson, R.L., Liu, Y., 1989. Diffusion of the interspecies electron carriers H_2 and formate in methanogenic ecosystems and its implications in the measurement of K_m for H_2 or formate uptake. Appl. Environ. Microbiol. 55, 1735–1741. https://doi.org/10.1128/aem.55.7.1735-1741.1989.

Braun, K., Gottschalk, G., 1981. Effect of molecular hydrogen and carbon dioxide on chemo-organotrophic growth of Acetobacterium woodii and Clostridium aceticum. Arch. Microbiol. 128, 294–298. https://doi.org/10.1007/BF00422533.

Buschhorn, H., Dürre, P., Gottschalk, G., 1989. Production and utilization of ethanol by the homoacetogen Acetobacterium woodii. Appl. Environ. Microbiol. 55, 1835–1840. https://doi.org/10.1128/AEM.55.7.1835-1840.1989.

Chatterjee, S., Huang, K.-W., 2020. Unrealistic energy and materials requirement for direct air capture in deep mitigation pathways. Nat. Commun. 11, 3287. https://doi.org/10.1038/s41467-020-17203-7.

Claassens, N.J., Bordanaba-Florit, G., Cotton, C.A.R., De Maria, A., Finger-Bou, M., Friedeheim, L., Giner-Laguarda, N., Munar-Palmer, M., Newell, W., Scarinci, G., Verbunt, J., de Vries, S.T., Yilmaz, S., Bar-Even, A., 2020. Replacing the Calvin cycle with the reductive glycine pathway in Cupriavidus necator. Metab. Eng. 62, 30–41. https://doi.org/10.1016/j.ymben.2020.08.004.

Claassens, N.J., Cotton, C.A.R., Kopljar, D., Bar-Even, A., 2019. Making quantitative sense of electromicrobial production. Nat Catal 2, 437–447. https://doi.org/10.1038/s41929-019-0272-0.

Claassens, N.J., Sánchez-Andrea, I., Sousa, D.Z., Bar-Even, A., 2018. Towards sustainable feedstocks: a guide to electron donors for microbial carbon fixation. Curr. Opin. Biotechnol. 50, 195–205. https://doi.org/10.1016/j.copbio.2018.01.019.

Cotton, C.A., Claassens, N.J., Benito-Vaquerizo, S., Bar-Even, A., 2020. Renewable methanol and formate as microbial feedstocks. Curr. Opin. Biotechnol. 62, 168–180. https://doi.org/10.1016/j.copbio.2019.10.002.

Cox, J., Mann, M., 2008. MaxQuant enables high peptide identification rates, individualized p.p.b.-range mass accuracies and proteome-wide protein quantification. Nat. Biotechnol. 26, 1367–1372. https://doi.org/10.1038/nbt.1511.

Demler, M., Weuster-Botz, D., 2011. Reaction engineering analysis of hydrogenotrophic production of acetic acid by Acetobacterium woodii. Biotechnol. Bioeng. 108, 470–474. https://doi.org/10.1002/bit.22935.
Diender, M., Stams, A.J.M., Sousa, D.Z., 2015. Pathways and bioenergetics of anaerobic carbon monoxide fermentation. Front. Microbiol. 6 https://doi.org/10.3389/fmicb.2015.01275.
Erian, A.M., Gibisch, M., Pflügl, S., 2018. Engineered *E. coli* W enables efficient 2,3-butanediol production from glucose and sugar beet molasses using defined minimal medium as economic basis. Microb. Cell Factories 17, 190. https://doi.org/10.1186/s12934-018-1038-0.
Fasihi, M., Efimova, O., Breyer, C., 2019. Techno-economic assessment of CO2 direct air capture plants. J. Clean. Prod. 224, 957–980. https://doi.org/10.1016/j.jclepro.2019.03.086.
Furdui, C., Ragsdale, S.W., 2000. The role of pyruvate ferredoxin oxidoreductase in pyruvate synthesis during autotrophic growth by the wood-ljungdahl pathway. J. Biol. Chem. 275, 28494–28499. https://doi.org/10.1074/jbc.M003291200.
Godley, Andrew R., Linnett, Paul E., Robinson, John P., 1990. The effect of carbon dioxide on the growth kinetics of fructose-limited chemostat cultures of Acetobacterium woodii DSM 1030. Arch. Microbiol. 154 https://doi.org/10.1007/BF00249170.
Goldberg, I., Rock, J.S., Ben-Bassat, A., Mateles, R.I., 1976. Bacterial yields on methanol, methylamine, formaldehyde, and formate. Biotechnol. Bioeng. 18, 1657–1668. https://doi.org/10.1002/bit.260181202.
Gonzalez de la Cruz, J., Machens, F., Messerschmidt, K., Bar-Even, A., 2019. Core catalysis of the reductive Glycine pathway demonstrated in yeast. ACS Synth. Biol. 8, 911–917. https://doi.org/10.1021/acssynbio.8b00464.
Haas, T., Krause, R., Weber, R., Demler, M., Schmid, G., 2018. Technical photosynthesis involving CO2 electrolysis and fermentation. Nat Catal 1, 32–39. https://doi.org/10.1038/s41929-017-0005-1.
Hardt, S., Stapf, S., Filmon, D.T., Birrell, J.A., Rüdiger, O., Fourmond, V., Léger, C., Plumeré, N., 2021. Reversible H2 oxidation and evolution by hydrogenase embedded in a redox polymer film. Nat Catal 4, 251–258. https://doi.org/10.1038/s41929-021-00586-1.
Hazeu, W., Donker, R.A., 1983. A continuous culture study of methanol and formate utilization by the yeast Pichia pastoris. Biotechnol. Lett. 5, 399–404. https://doi.org/10.1007/BF00131280.
Hermann, M., Teleki, A., Weitz, S., Niess, A., Freund, A., Bengelsdorf, F.R., Takors, R., 2020. Electron availability in CO_2 , CO and H_2 mixtures constrains flux distribution, energy management and product formation in *Clostridium ljungdahlii*. Microb. Biotechnol. 13, 1831–1846. https://doi.org/10.1111/1751-7915.13625.
Hofer, A., Kamravamanesh, D., Bona-Lovasz, J., Limbeck, A., Lendl, B., Herwig, C., Fricke, J., 2018. Prediction of filamentous process performance attributes by CSL quality assessment using mid-infrared spectroscopy and chemometrics. J. Biotechnol. 265, 93–100. https://doi.org/10.1016/j.jbiotec.2017.11.010.
Hoffmeister, S., Gerdom, M., Bengelsdorf, F.R., Linder, S., Flüchter, S., Öztürk, H., Blümke, W., May, A., Fischer, R.-J., Bahl, H., Dürre, P., 2016. Acetone production with metabolically engineered strains of Acetobacterium woodii. Metab. Eng. 36, 37–47. https://doi.org/10.1016/j.ymben.2016.03.001.
Huang, H., Wang, S., Moll, J., Thauer, R.K., 2012. Electron bifurcation involved in the energy metabolism of the acetogenic bacterium Moorella thermoacetica growing on glucose or H2 plus CO2. J. Bacteriol. 194, 3689–3699. https://doi.org/10.1128/JB.00385-12.
Jones, S.W., Fast, A.G., Carlson, E.D., Wiedel, C.A., Au, J., Antoniewicz, M.R., Papoutsakis, E.T., Tracy, B.P., 2016. CO2 fixation by anaerobic non-photosynthetic mixotrophy for improved carbon conversion. Nat. Commun. 7, 12800. https://doi.org/10.1038/ncomms12800.
Kantzow, C., Mayer, A., Weuster-Botz, D., 2015. Continuous gas fermentation by Acetobacterium woodii in a submerged membrane reactor with full cell retention. J. Biotechnol. 212, 11–18. https://doi.org/10.1016/j.jbiotec.2015.07.020.
Karmann, S., Follonier, S., Egger, D., Hebel, D., Panke, S., Zinn, M., 2017. Tailor-made PAT platform for safe syngas fermentations in batch, fed-batch and chemostat mode with Rhodospirillum rubrum. Microb. Biotechnol. 10, 1365–1375. https://doi.org/10.1111/1751-7915.12727.
Kelly, D.P., Baker, S.C., Trickett, J., Davey, M., Murrell, J.C., 1994. Methanesulphonate utilization by a novel methylotrophic bacterium involves an unusual monooxygenase. Microbiology 140, 1419–1426. https://doi.org/10.1099/00221287-140-6-1419.
Kim, S., Lindner, S.N., Aslan, S., Yishai, O., Wenk, S., Schann, K., Bar-Even, A., 2020. Growth of E. coli on formate and methanol via the reductive glycine pathway. Nat. Chem. Biol. 16, 538–545. https://doi.org/10.1038/s41589-020-0473-5.
Klamt, S., Saez-Rodriguez, J., Gilles, E.D., 2007. Structural and functional analysis of cellular networks with CellNetAnalyzer. BMC Syst. Biol. 1, 2. https://doi.org/10.1186/1752-0509-1-2.
Koch, S., Kohrs, F., Lahmann, P., Bissinger, T., Wendschuh, S., Benndorf, D., Reichl, U., Klamt, S., 2019. RedCom: a strategy for reduced metabolic modeling of complex microbial communities and its application for analyzing experimental datasets from anaerobic digestion. PLoS Comput. Biol. 15, e1006759 https://doi.org/10.1371/journal.pcbi.1006759.
Köpke, M., Simpson, S.D., 2020. Pollution to products: recycling of 'above ground' carbon by gas fermentation. Curr. Opin. Biotechnol. 65, 180–189. https://doi.org/10.1016/j.copbio.2020.02.017.
Kremp, F., Poehlein, A., Daniel, R., Müller, V., 2018. Methanol metabolism in the acetogenic bacterium Acetobacterium woodii. Environ. Microbiol. 20, 4369–4384. https://doi.org/10.1111/1462-2920.14356.
Kremp, F., Roth, J., Müller, V., 2020. The *Sporomusa* type Nfn is a novel type of electron-bifurcating transhydrogenase that links the redox pools in acetogenic bacteria. Sci. Rep. 10, 14872. https://doi.org/10.1038/s41598-020-71038-2.
Li, H., Opgenorth, P.H., Wernick, D.G., Rogers, S., Wu, T.-Y., Higashide, W., Malati, P., Huo, Y.-X., Cho, K.M., Liao, J.C., 2012. Integrated electromicrobial conversion of CO2 to higher alcohols. Science 335, 1596. https://doi.org/10.1126/science.1217643, 1596.
Liew, F., Martin, M.E., Tappel, R.C., Heijstra, B.D., Mihalcea, C., Köpke, M., 2016. Gas fermentation—a flexible platform for commercial scale production of low-carbon-fuels and chemicals from waste and renewable feedstocks. Front. Microbiol. 7 https://doi.org/10.3389/fmicb.2016.00694.
Litty, D., Müller, V., 2021. Butyrate production in the acetogen *Eubacterium limosum* is dependent on the carbon and energy source. Microb. Biotechnol. 1751–7915, 13779. https://doi.org/10.1111/1751-7915.13779.
Loubiere, P., Gros, E., Paquet, V., Lindley, N.D., 1992. Kinetics and physiological implications of the growth behaviour of Eubacterium limosum on glucose/methanol mixtures. J. Gen. Microbiol. 138, 979–985. https://doi.org/10.1099/00221287-138-5-979.
Love, M.I., Huber, W., Anders, S., 2014. Moderated estimation of fold change and dispersion for RNA-seq data with DESeq2. Genome Biol. 15, 550. https://doi.org/10.1186/s13059-014-0550-8.
Maru, B.T., Munasinghe, P.C., Gilary, H., Jones, S.W., Tracy, B.P., 2018. Fixation of CO2 and CO on a diverse range of carbohydrates using anaerobic, non-photosynthetic mixotrophy. FEMS (Fed. Eur. Microbiol. Soc.) Microbiol. Lett. 365 https://doi.org/10.1093/femsle/fny039.
Molitor, B., Marcellin, E., Angenent, L.T., 2017. Overcoming the energetic limitations of syngas fermentation. Curr. Opin. Chem. Biol. 41, 84–92. https://doi.org/10.1016/j.cbpa.2017.10.003.
Moon, J., Dönig, J., Kramer, S., Poehlein, A., Daniel, R., Müller, V., 2021. Formate metabolism in the acetogenic bacterium *Acetobacterium woodii*. Environ. Microbiol. 1462–2920, 15598. https://doi.org/10.1111/1462-2920.15598.
Müller, V., 2019. New horizons in acetogenic conversion of one-carbon substrates and biological hydrogen storage. Trends Biotechnol. https://doi.org/10.1016/j.tibtech.2019.05.008.
Nguyen, N.-P.-T., Raynaud, C., Meynial-Salles, I., Soucaille, P., 2018. Reviving the Weizmann process for commercial n-butanol production. Nat. Commun. 9. https://doi.org/10.1038/s41467-018-05661-z.
Nissen, T.L., Schulze, U., Nielsen, J., Villadsen, J., 1997. Flux distributions in anaerobic, glucose-limited continuous cultures of Saccharomyces cerevisiae. Microbiology 143, 203–218. https://doi.org/10.1099/00221287-143-1-203.
Novak, K., Neuendorf, C.S., Kofler, I., Kieberger, N., Klamt, S., Pflügl, S., 2021. Blending industrial blast furnace gas with H2 enables Acetobacterium woodii to efficiently co-utilize CO, CO2 and H2. Bioresour. Technol. 323, 124573. https://doi.org/10.1016/j.biortech.2020.124573.
Panich, J., Fong, B., Singer, S.W., 2021. Metabolic engineering of Cupriavidus necator H16 for sustainable biofuels from CO2. Trends Biotechnol. 39, 412–424. https://doi.org/10.1016/j.tibtech.2021.01.001.
Patro, R., Duggal, G., Love, M.I., Irizarry, R.A., Kingsford, C., 2017. Salmon provides fast and bias-aware quantification of transcript expression. Nat. Methods 14, 417–419. https://doi.org/10.1038/nmeth.4197.
Perez-Riverol, Y., Csordas, A., Bai, J., Bernal-Llinares, M., Hewapathirana, S., Kundu, D. J., Inuganti, A., Griss, J., Mayer, G., Eisenacher, M., Pérez, E., Uszkoreit, J., Pfeuffer, J., Sachsenberg, T., Yılmaz, Ş., Tiwary, S., Cox, J., Audain, E., Walzer, M., Jarnuczak, A.F., Ternent, T., Brazma, A., Vizcaíno, J.A., 2019. The PRIDE database and related tools and resources in 2019: improving support for quantification data. Nucleic Acids Res. 47, D442–D450. https://doi.org/10.1093/nar/gky1106.
Pertea, G., Pertea, M., 2020. GFF utilities: GffRead and GffCompare. F1000Res 9, 304. https://doi.org/10.12688/f1000research.23297.2.
Pluschkell, S.B., Flickinger, M.C., 2002. Dissimilation of [13C]methanol by continuous cultures of Bacillus methanolicus MGA3 at 50 °C studied by 13C NMR and isotope-ratio mass spectrometry. Microbiology 148, 3223–3233. https://doi.org/10.1099/00221287-148-10-3223.
Poehlein, A., Schmidt, S., Kaster, A.-K., Goenrich, M., Vollmers, J., Thürmer, A., Bertsch, J., Schuchmann, K., Voigt, B., Hecker, M., Daniel, R., Thauer, R.K., Gottschalk, G., Müller, V., 2012. An ancient pathway combining carbon dioxide fixation with the generation and utilization of a sodium Ion gradient for ATP synthesis. PloS One 7, e33439. https://doi.org/10.1371/journal.pone.0033439.
R Core Team, 2013. R: A Language and Environment for Statistical Computing.
Realmonte, G., Drouet, L., Gambhir, A., Glynn, J., Hawkes, A., Köberle, A.C., Tavoni, M., 2019. An inter-model assessment of the role of direct air capture in deep mitigation pathways. Nat. Commun. 10, 3277. https://doi.org/10.1038/s41467-019-10842-5.
Richter, H., Molitor, B., Wei, H., Chen, W., Aristilde, L., Angenent, L.T., 2016. Ethanol Production in Syngas-Fermenting Clostridium Ljungdahlii Is Controlled by Thermodynamics rather than by Enzyme Expression 9, pp. 2392–2399. https://doi.org/10.1039/c6ee01108j.
Rintala, E., Wiebe, M.G., Tamminen, A., Ruohonen, L., Penttilä, M., 2008. Transcription of hexose transporters of Saccharomyces cerevisiae is affected by change in oxygen provision. BMC Microbiol. 8, 53. https://doi.org/10.1186/1471-2180-8-53.
Rittmann, S., Seifert, A., Herwig, C., 2012. Quantitative analysis of media dilution rate effects on Methanothermobacter marburgensis grown in continuous culture on H2 and CO2. Biomass Bioenergy 36, 293–301. https://doi.org/10.1016/j.biombioe.2011.10.038.
Schendel, F.J., Bremmon, C.E., Flickinger, M.C., Hanson, R.S., 1990. L-lysine production at 50°C by mutants of a newly isolated and characterized methylotrophic Bacillus sp. Appl. Environ. Microbiol. 56, 8.

Schoelmerich, M.C., Katsyv, A., Sung, W., Mijic, V., Wiechmann, A., Kottenhahn, P., Baker, J., Minton, N.P., Müller, V., 2018. Regulation of lactate metabolism in the acetogenic bacterium *Acetobacterium woodii*. Environ. Microbiol. 20, 4587–4595. https://doi.org/10.1111/1462-2920.14412.

Schuchmann, K., Müller, V., 2013. Direct and reversible hydrogenation of CO2 to formate by a bacterial carbon dioxide reductase. Science 342, 1382–1385. https://doi.org/10.1126/science.1244758.

Schuchmann, K., Müller, V., 2014. Autotrophy at the thermodynamic limit of life: a model for energy conservation in acetogenic bacteria. Nat. Rev. Microbiol. 12, 809–821. https://doi.org/10.1038/nrmicro3365.

Schwarz, F.M., Ciurus, S., Jain, S., Baum, C., Wiechmann, A., Basen, M., Müller, V., 2020. Revealing formate production from carbon monoxide in wild type and mutants of Rnf- and Ech-containing acetogens, *Acetobacterium woodii* and *Thermoanaerobacter kivui*. Microb. Biotechnol. 13, 2044–2056. https://doi.org/10.1111/1751-7915.13663.

Schwarz, F.M., Müller, V., 2020. Whole-cell biocatalysis for hydrogen storage and syngas conversion to formate using a thermophilic acetogen. Biotechnol. Biofuels 13, 32. https://doi.org/10.1186/s13068-020-1670-x.

Shay, L.K., Hunt, H.R., Wegner, G.H., 1987. High-productivity fermentation process for cultivating industrial microorganisms. J. Ind. Microbiol. 2, 79–85. https://doi.org/10.1007/BF01569506.

Soneson, C., Love, M.I., Robinson, M.D., 2016. Differential analyses for RNA-seq: transcript-level estimates improve gene-level inferences. F1000Res 4, 1521. https://doi.org/10.12688/f1000research.7563.2.

Song, Y., Lee, J.S., Shin, J., Lee, G.M., Jin, S., Kang, S., Lee, J.-K., Kim, D.R., Lee, E.Y., Kim, S.C., Cho, S., Kim, D., Cho, B.-K., 2020. Functional cooperation of the glycine synthase-reductase and Wood–Ljungdahl pathways for autotrophic growth of Clostridium drakei. Proc. Natl. Acad. Sci. Unit. States Am. https://doi.org/10.1073/pnas.1912289117, 201912289.

Trifunović, D., Berghaus, N., Müller, V., 2020. Growth of the acetogenic bacterium Acetobacterium woodii by dismutation of acetaldehyde to acetate and ethanol. Environmental Microbiology Reports 12, 58–62. https://doi.org/10.1111/1758-2229.12811.

Tschech, A., Pfennig, N., 1984. Growth yield increase linked to caffeate reduction in Acetobacterium woodii. Arch. Microbiol. 137, 163–167. https://doi.org/10.1007/BF00414460.

Tyanova, S., Temu, T., Cox, J., 2016a. The MaxQuant computational platform for mass spectrometry-based shotgun proteomics. Nat. Protoc. 11, 2301–2319. https://doi.org/10.1038/nprot.2016.136.

Tyanova, S., Temu, T., Sinitcyn, P., Carlson, A., Hein, M.Y., Geiger, T., Mann, M., Cox, J., 2016b. The Perseus computational platform for comprehensive analysis of (prote) omics data. Nat. Methods 13, 731–740. https://doi.org/10.1038/nmeth.3901.

Valgepea, K., de Souza Pinto Lemgruber, R., Abdalla, T., Binos, S., Takemori, N., Takemori, A., Tanaka, Y., Tappel, R., Köpke, M., Simpson, S.D., Nielsen, L.K., Marcellin, E., 2018. H2 drives metabolic rearrangements in gas-fermenting Clostridium autoethanogenum. Biotechnol. Biofuels 11, 55. https://doi.org/10.1186/s13068-018-1052-9.

Valgepea, K., de Souza Pinto Lemgruber, R., Meaghan, K., Palfreyman, R.W., Abdalla, T., Heijstra, B.D., Behrendorff, J.B., Tappel, R., Köpke, M., Simpson, S.D., Nielsen, L.K., Marcellin, E., 2017. Maintenance of ATP homeostasis triggers metabolic shifts in gas-fermenting acetogens. Cell Systems 4, 505–515. https://doi.org/10.1016/j.cels.2017.04.008.

Van Hecke, W., Bockrath, R., De Wever, H., 2019. Effects of moderately elevated pressure on gas fermentation processes. Bioresour. Technol. 293, 122129. https://doi.org/10.1016/j.biortech.2019.122129.

Vees, C.A., Neuendorf, C.S., Pflügl, S., 2020. Towards continuous industrial bioprocessing with solventogenic and acetogenic clostridia: challenges, progress and perspectives. J. Ind. Microbiol. Biotechnol. 47, 753–787. https://doi.org/10.1007/s10295-020-02296-2.

von Kamp, A., Thiele, S., Hädicke, O., Klamt, S., 2017. Use of CellNetAnalyzer in biotechnology and metabolic engineering. J. Biotechnol. 261, 221–228. https://doi.org/10.1016/j.jbiotec.2017.05.001.

Wendisch, V.F., Brito, L.F., Gil Lopez, M., Hennig, G., Pfeifenschneider, J., Sgobba, E., Veldmann, K.H., 2016. The flexible feedstock concept in Industrial Biotechnology: metabolic engineering of Escherichia coli, Corynebacterium glutamicum, Pseudomonas, Bacillus and yeast strains for access to alternative carbon sources. J. Biotechnol. 234, 139–157. https://doi.org/10.1016/j.jbiotec.2016.07.022.

Wiechmann, A., Ciurus, S., Oswald, F., Seiler, V.N., Müller, V., 2020. It does not always take two to tango: "Syntrophy" via hydrogen cycling in one bacterial cell. ISME J. https://doi.org/10.1038/s41396-020-0627-1.

Wolin, M.J., Miller, T.L., Collins, M.D., Lawson, P.A., 2003. Formate-Dependent Growth and Homoacetogenic Fermentation by a Bacterium from Human Feces: Description of Bryantella formatexigens gen. nov., sp. nov. AEM 69, 6321–6326. https://doi.org/10.1128/AEM.69.10.6321-6326.2003.

Yishai, O., Lindner, S.N., Gonzalez de la Cruz, J., Tenenboim, H., Bar-Even, A., 2016. The formate bio-economy. Curr. Opin. Chem. Biol. 35, 1–9. https://doi.org/10.1016/j.cbpa.2016.07.005.

Zelcbuch, L., Lindner, S.N., Zegman, Y., Vainberg Slutskin, I., Antonovsky, N., Gleizer, S., Milo, R., Bar-Even, A., 2016. Pyruvate formate-lyase enables efficient growth of *Escherichia coli* on acetate and formate. Biochemistry 55, 2423–2426. https://doi.org/10.1021/acs.biochem.6b00184.

Zhu, A., Ibrahim, J.G., Love, M.I., 2019. Heavy-tailed prior distributions for sequence count data: removing the noise and preserving large differences. Bioinformatics 35, 2084–2092. https://doi.org/10.1093/bioinformatics/bty895.